AEDC-TDR-64-277

LAMINAR BOUNDARY-LAYER SEPARATION ON FLARED BODIES AT SUPERSONIC AND HYPERSONIC SPEEDS

By

J. Don Gray
von Kármán Gas Dynamics Facility
ARO, Inc.

TECHNICAL DOCUMENTARY REPORT NO. AEDC-TDR-64-277

January 1965

Program Element 62405334/8953, Task 895303

(Prepared under Contract No. AF 40(600)-1000 by ARO, Inc., contract operator of AEDC, Arnold Air Force Station, Tenn.)

ARNOLD ENGINEERING DEVELOPMENT CENTER
AIR FORCE SYSTEMS COMMAND
UNITED STATES AIR FORCE

NOTICES

Qualified requesters may obtain copies of this report from DDC, Cameron Station, Alexandria, Va. Orders will be expedited if placed through the librarian or other staff member designated to request and receive documents from DDC.

When Government drawings, specifications or other data are used for any purpose other than in connection with a definitely related Government procurement operation, the United States Government thereby incurs no responsibility nor any obligation whatsoever; and the fact that the Government may have formulated, furnished, or in any way supplied the said drawings, specifications, or other data, is not to be regarded by implication or otherwise as in any manner licensing the holder or any other person or corporation, or conveying any rights or permission to manufacture, use, or sell any patented invention that may in any way be related thereto.

UNCLASSIFIED
Security Classification

DOCUMENT CONTROL DATA - R&D

(Security classification of title, body of abstract and indexing annotation must be entered when the overall report is classified)

1. ORIGINATING ACTIVITY *(Corporate author)* ARO, Inc. Arnold AF Station, Tennessee	2a. REPORT SECURITY CLASSIFICATION UNCLASSIFIED 2b. GROUP N/A

3. REPORT TITLE LAMINAR BOUNDARY-LAYER SEPARATION ON FLARED BODIES AT SUPERSONIC AND HYPERSONIC SPEEDS

4. DESCRIPTIVE NOTES *(Type of report and inclusive dates)*
N/A

5. AUTHOR(S) *(Last name, first name, initial)*
Gray, J. Don

6. REPORT DATE	7a. TOTAL NO. OF PAGES	7b. NO. OF REFS
January 1965	58	17

8a. CONTRACT OR GRANT NO.	9a. ORIGINATOR'S REPORT NUMBER(S)
AF40(600)-1000 b. PROJECT NO. 8953 c. Program Element 62405334 d. Task 895303	AEDC-TDR-64-277 9b. OTHER REPORT NO(S) *(Any other numbers that may be assigned this report)* None

10. AVAILABILITY/LIMITATION NOTICES
None

11. SUPPLEMENTARY NOTES	12. SPONSORING MILITARY ACTIVITY
	Arnold Engineering Development Center, Arnold AF Station, Tenn.

13. ABSTRACT

Experiments at supersonic speeds and at Mach 8 were conducted to determine the conditions which govern the extent of shock-induced laminar flow separations on axisymmetric configurations at zero yaw and without heat transfer. From an extensive correlation of surface pressure data and schlieren photographs, it is shown that the extent of reverse flow is essentially a function of the ratio of the wetted length to the flare divided by the laminar boundary thickness there. As a result, the relative extent of laminar flow separation decreases with a unit Reynolds number increase and grows through an increase in Mach number. Finally, increasing the flare angle increases the length of the reverse flow region.

DD FORM 1 JAN 64 1473

UNCLASSIFIED
Security Classification

14. KEY WORDS	LINK A		LINK B		LINK C	
	ROLE	WT	ROLE	WT	ROLE	WT

INSTRUCTIONS

1. ORIGINATING ACTIVITY: Enter the name and address of the contractor, subcontractor, grantee, Department of Defense activity or other organization *(corporate author)* issuing the report,

2*a*. REPORT SECURITY CLASSIFICATION: Enter the overall security classification of the report. Indicate whether "Restricted Data" is included. Marking is to be in accordance with appropriate security regulations.

2*b*. GROUP: Automatic downgrading is specified in DoD Directive 5200.10 and Armed Forces Industrial Manual. Enter the group number. Also, when applicable, show that optional markings have been used for Group 3 and Group 4 as authorized.

3. REPORT TITLE: Enter the complete report title in all capital letters. Titles in all cases should be unclassified. If a meaningful title cannot be selected without classification, show title classification in all capitals in parenthesis immediately following the title.

4. DESCRIPTIVE NOTES: If appropriate, enter the type of report, e.g., interim, progress, summary, annual, or final. Give the inclusive dates when a specific reporting period is covered.

5. AUTHOR(S): Enter the name(s) of author(s) as shown on or in the report. Enter last name, first name, middle initial. If military, show rank and branch of service. The name of the principal author is an absolute minimum requirement.

6. REPORT DATE: Enter the date of the report as day, month, year; or month, year. If more than one date appears on the report, use date of publication.

7*a*. TOTAL NUMBER OF PAGES: The total page count should follow normal pagination procedures, i.e., enter the number of pages containing information.

7*b*. NUMBER OF REFERENCES: Enter the total number of references cited in the report.

8*a*. CONTRACT OR GRANT NUMBER: If appropriate, enter the applicable number of the contract or grant under which the report was written.

8*b*, 8*c*, & 8*d*. PROJECT NUMBER: Enter the appropriate military department identification, such as project number, subproject number, system numbers, task number, etc.

9*a*. ORIGINATOR'S REPORT NUMBER(S): Enter the official report number by which the document will be identified and controlled by the originating activity. This number must be unique to this report.

9*b*. OTHER REPORT NUMBER(S): If the report has been assigned any other report numbers *(either by the originator or by the sponsor)*, also enter this number(s).

10. AVAILABILITY/LIMITATION NOTICES: Enter any limitations on further dissemination of the report, other than those imposed by security classification, using standard statements such as:

(1) "Qualified requesters may obtain copies of this report from DDC."

(2) "Foreign announcement and dissemination of this report by DDC is not authorized."

(3) "U. S. Government agencies may obtain copies of this report directly from DDC. Other qualified DDC users shall request through

_____."

(4) "U. S. military agencies may obtain copies of this report directly from DDC. Other qualified users shall request through

_____."

(5) "All distribution of this report is controlled. Qualified DDC users shall request through

_____."

If the report has been furnished to the Office of Technical Services, Department of Commerce, for sale to the public, indicate this fact and enter the price, if known.

11. SUPPLEMENTARY NOTES: Use for additional explanatory notes.

12. SPONSORING MILITARY ACTIVITY: Enter the name of the departmental project office or laboratory sponsoring *(paying for)* the research and development. Include address.

13. ABSTRACT: Enter an abstract giving a brief and factual summary of the document indicative of the report, even though it may also appear elsewhere in the body of the technical report. If additional space is required, a continuation sheet shall be attached.

It is highly desirable that the abstract of classified reports be unclassified. Each paragraph of the abstract shall end with an indication of the military security classification of the information in the paragraph, represented as *(TS), (S), (C), or (U)*.

There is no limitation on the length of the abstract. However, the suggested length is from 150 to 225 words.

14. KEY WORDS: Key words are technically meaningful terms or short phrases that characterize a report and may be used as index entries for cataloging the report. Key words must be selected so that no security classification is required. Identifiers, such as equipment model designation, trade name, military project code name, geographic location, may be used as key words but will be followed by an indication of technical context. The assignment of links, rules, and weights is optional.

LAMINAR BOUNDARY-LAYER SEPARATION ON FLARED BODIES AT SUPERSONIC AND HYPERSONIC SPEEDS

By

J. Don Gray

von Kármán Gas Dynamics Facility

ARO, Inc.

a subsidiary of Sverdrup and Parcel, Inc.

January 1965

ARO Project No. VA2316

ABSTRACT

Experiments at supersonic speeds and at Mach 8 were conducted to determine the conditions which govern the extent of shock-induced laminar flow separations on axisymmetric configurations at zero yaw and without heat transfer. From an extensive correlation of surface pressure data and schlieren photographs, it is shown that the extent of reverse flow is essentially a function of the ratio of the wetted length to the flare divided by the laminar boundary thickness there. As a result, the relative extent of laminar flow separation decreases with a unit Reynolds number increase and grows through an increase in Mach number. Finally, increasing the flare angle increases the length of the reverse flow region.

PUBLICATION REVIEW

This report has been reviewed and publication is approved.

Larry R. Walter
1st Lt, USAF
Gas Dynamics Division
DCS/Research

Donald R. Eastman, Jr.
DCS/Research

CONTENTS

TABLE

ILLUSTRATIONS

NOMENCLATURE

C_p	Pressure coefficient, $(p - p_o)/q_o$
L	Frustum axial length, in.
M	Mach number
p	Static pressure, psia
p'	Pitot pressure, psia
q	Dynamic pressure, psia
R	Radius of centerbody, in.
Re_x	Reynolds number (based on free-stream conditions and length x)
T	Temperature, °F
U	Velocity, ft/sec
x	Wetted length, in.
Δx	Incremental length $(x - x_s)$, in.
x*	Axial distance downstream from start of frustum, in.
y	Distance normal to surface, in.
α	Angle between flat plate and free stream, deg
δ	Boundary-layer thickness, in.
η	Normal distance parameter, $(y/x)\sqrt{Re_x}$
η_v	Boundary-layer thickness parameter, $(\delta/x)\sqrt{Re_x}$
θ	Frustum semi-angle, deg
ξ	Axial distance upstream from start of frustum, in.
$\xi(\theta)$	Correlation parameter for extent of reverse flow, see Eq. (3)
ϕ	Angle between edge of reverse flow region and axis of symmetry, deg
ψ	Pitot probe angle with respect to model, deg

SUBSCRIPTS

aw	Adiabatic wall
c	Corner formed by frustum and cylinder

o	Beginning of interaction near separation
p	Plateau region of constant pressure
s	Shoulder formed by nose and cylinder
t	Total
tr	Beginning of transition
w	Wall
δ	Outer edge of boundary layer
∞	Undisturbed free-stream

1.0 INTRODUCTION

The problem of shock-induced flow separation on two-dimensional configurations has been extensively investigated (Refs. 1 through 12), whereas axisymmetric configurations have naturally received less attention (Refs. 13 through 15) since the fundamental problem in plane flow is not yet fully understood. Despite the considerable interest in this subject over the past decade, no straightforward solution exists for the general problem of separation ahead of a flap or flare. Although a large electronic computer is required, the recent work of Lees and Reeves (Ref. 16) appears to satisfactorily account for this complete interaction process in two-dimensional flow.

Since no simple working criteria existed for a definition of the degree of flow separation to be expected on axisymmetric configurations, the present research was undertaken simply to define the important parameters governing the extent of the reverse flow region.

2.0 APPARATUS

2.1 WIND TUNNELS

The experiments were conducted in the von Karman Facility Gas Dynamic Wind Tunnels: Supersonic (A) and (D) and Hypersonic (B) and (E). Tunnels A and B are continuous-flow, variable-density wind tunnels with 40- x 40-in.-square and 50-in.-diam test sections, respectively. Tunnel A operates from Mach 1.5 to 6 at maximum stagnation pressures from 29 to 200 psia, respectively. Tunnel B has a Mach 8 contoured axisymmetric nozzle and operates from about 100 to 900 psia. Test units D and E are intermittent, variable-density wind tunnels with 12- x 12-in. test sections. Tunnel D operates from Mach 1.5 to 5 at stagnation pressures from 5 to 60 psia, and Tunnel E operates from Mach 5 to 8 with maximum stagnation pressures from 400 to 1600 psia, respectively. Further details of these wind tunnels may be found in Ref. 17.

2.2 MODELS

A 7-in.-diam hollow cylinder (HC), threaded at one end, was used as a basic centerbody for the 10-deg sharp cone (10S), 15-deg blunt

Manuscript received December 1964.

cone (15B), and sharp lip (HC) noses (see Fig. 1a). A typical configuration, for example the sharp lip hollow cylinder with a 20-deg flare, is referred to as HC-20. Other configurations are treated similarly. Forty surface pressure orifices were installed, along a ray, between an inner and outer shell over a 17-in. region. Three frustums (10-, 15- and 20-deg) could be slipped onto the cylinder; twenty orifices were provided on the 10- and 20-deg flares and forty orifices on the 15-deg flare. The flares were connected to a remotely operated hydraulic piston, as shown in Fig. 1b, to vary the centerbody length during tunnel operation. These models were provided by the AVCO Corporation of Wilmington, Massachusetts.

A 1.0-in.-diam hollow cylinder with a sharp lip and an adjustable flare was provided for flow visualization studies in Tunnels D and E.

2.3 INSTRUMENTATION

The surface pressures were measured with a pressure-scanning system utilizing 1- and 15-psia capacity transducers with three ranges calibrated to read approximately 20, 50 and 100 percent of rated capacity at full scale. A near vacuum reference was used. The precision of the system is estimated to be about 2 percent of the full-scale pressure for the range being considered.

The pitot pressures obtained during the boundary-layer measurement phase were measured with a 15-psid capacity transducer (vacuum reference) having six ranges calibrated to read about 2, 5, 10, 20, 50 and 100 percent of rated capacity at full scale. The precision of this system is estimated to be about 1 percent of the full-scale pressure for the corresponding range. The vertical-survey probe readout system used for the boundary-layer measurements provided a height reading with a precision which is considered to be better than 0.001-in.

3.0 DISCUSSION OF RESULTS

3.1 SCOPE OF TESTS

The range of the main test conditions for the various configurations is summarized in Table 1. All of the tests were conducted with the models at zero yaw and with the model wall temperature in equilibrium with the flow.

3.2 TURBULENT FLOW EFFECTS

Since the discussion will be, primarily, on the effects of flow separation on the surface pressure distribution of axisymmetric configurations, it is proper to consider first the character of some typical pressure distributions in supersonic flow without laminar boundary-layer separation. The pressure distribution on a conical frustum (HC-20) at Mach 3, 4, and 5 is compared with theory in Fig. 2a. Schlieren photographs at Mach 4 and 5 show no evidence of reverse flow regions and illustrate the turbulent state of the boundary layer. Cylinder pressures were constant all the way to the corner formed by the flare; thus, no measurable turbulent separation was present. Consequently, the pressure distribution near the corner of a frustum is modified by the turbulent boundary layer such that the location of the corner is effectively shifted downstream. Strict comparisons in Fig. 2a will show that the actual pressure gradient downstream of the peak value is considerably reduced from that indicated by theory at the corner in each case.

The centerbody and frustum pressure distributions for the 10-deg sharp cone-cylinder with a 20-deg flare (10S-20) are presented in Figs. 2b and c. Excellent agreement is noted in Fig. 2b between theory and experiment on the centerbody at each Mach number. Although the initial rise to a peak appears (in Fig. 2c) noticeably softened relative to that for the HC-20 frustum, the distributions are otherwise qualitatively alike. The thicker turbulent boundary layers, shown by the accompanying schlieren photographs in Fig. 2c, are obviously responsible for the softening effect.

Because of the influence of nose bluntness on boundary-layer transition and on the local unit Reynolds number, no results were obtained with a turbulent boundary layer approaching the 20-deg frustum when combined with the 15-deg blunted cone-cylinder (configuration 15B-20). However, a reasonable approximation of negligible flow separation is provided by the data shown in Fig. 2d for $M_\infty = 4$ and at a maximum unit Reynolds number of 0.55×10^6 per inch. The schlieren photograph shows that a small reverse flow region (about 1R in length) exists, and as well the centerbody pressure distribution shows a small effect of flow separation. The flare pressure distribution for the initial rise (0 to about 0.6R) is qualitatively the same as that for the other configurations, whereas on the downstream end the pressures rise instead of fall. This latter trend is characteristic of shear layer effects as shown in Ref. 18, from which a qualitative estimate of the inviscid distribution was derived.

In view of the similarity of results from each of these configurations, it may be concluded that the classical inviscid viewpoint of judging

pressure distributions near the corner of a frustum is not representative of experimental results with turbulent boundary layers. Inasmuch as the effects observed are opposite to those associated with radial shear gradients (Ref. 18 and see Fig. 2c), it must be that the corner gradient is the result of an interaction between the inviscid flow and the turbulent boundary layer.

3.3 LAMINAR FLOW SEPARATION FEATURES

Early in this research it was realized that a distinct and reliable determination of the beginning of boundary-layer transition on the flare, in the neighborhood of flow reattachment, is virtually impossible to achieve when the flare angle is over about 10 or 15 deg. Consequently, it was not possible to distinguish between pure laminar and transitional separations when transition was very near to the reattachment zone, despite its demonstrated importance in Ref. 2. As a result, a laminar flow separation is defined in this report as the separation of a laminar boundary layer from the wall upstream of a flare or flap and which remains clearly laminar until its intersection with the deflected surface based upon both schlieren photographs and the pressure distribution indicating an appreciable constant pressure region upstream of the flare. As a matter of record it should be recalled that Chapman, Kuehn, and Larson (in Ref. 2) defined pure laminar separations as those where transition is downstream of the reattachment zone and transitional separations as those where transition is anywhere between separation and reattachment.

The general characteristics of a shock-induced, laminar boundary-layer separation are indicated by the results in Fig. 3. Briefly, the flare pressure rise is considered to propagate upstream through the subsonic region of the boundary layer to a position of equilibrium between the wall shear and the external, inviscid flow. These conditions sustain a region of steady recirculating flow. It is this region, containing the reversed flow, that is particularly evident in the schlieren photographs, i. e., the white region upstream of the flare. The sketch more clearly indicates the region, and the corresponding influence of the separation, upon the surface pressure distribution above. The interaction process is noted to begin at about $\xi/R = 4$ and to end near $\xi/R = 3$, but the separation location is not so obviously located. Previous investigations, Refs. 2 and 12, have shown it to be approximately midway between the two locations. Because the location of separation requires additional measurements (oil flow, Stanton tubes, etc.), the beginning of the interaction was chosen as the location defining the extent of flow separation in this research. This location was also found to correspond

approximately to the point of intersection of an extrapolation of the outer edge of the reverse flow region with the body surface; thus, schlieren photographs can be directly related to the pressure measurements.

Downstream of the corner, the reattachment process is considered to begin when the flare pressure starts a rapid but smooth rise from the plateau pressure level. This always begins some distance upstream of the location where the outer edge of the reverse flow region intersects the flare surface. Beyond this position ($x^*/R \sim 0.8$) the pressure rises smoothly to a value about equal to the peak inviscid level indicated by theory, then begins the pressure decay characteristic of frustums in uniform supersonic flow. This latter part of the flare pressure rise, where the rate of change of the pressure gradient, d^2p/dx^2, becomes increasingly negative, is functionally the same distribution as was obtained with an attached turbulent boundary layer (see Fig. 2c). Therefore, this suggests that the reattachment process for laminar flow separation begins where the pressure starts to rise from the plateau and ends about when the flare pressure gradient reaches a maximum.

Pitot pressure profiles included in Fig. 3 illustrate not only the height of the reverse flow and the similarity of profiles along that region (locations A through D), but also that the reattachment process is essentially complete at Station E. This latter statement is based on the smooth rise in pitot pressure with height increase, the variation shown being characteristic of a laminar profile (with constant static pressure through the layer). Finally, the profile at Station F indicates that a reduction in boundary-layer thickness occurred along with a Mach number decrease (nearly doubled pitot pressure) in the region downstream of reattachment.

3.4 LAMINAR BOUNDARY-LAYER CHARACTERISTICS

Because the boundary-layer dimensions are such an important variable in any separation and mixing process, pitot profile measurements were made on each of the basic axisymmetric configurations, as indicated in Table 1, at one or more stations.

As a matter of interest, the data presented in Fig. 3 for Stations A and C have been converted to non-dimensional coordinates, η and M/M_δ, in Fig. 4a. It should be observed that the Blasius-type parameter, η, is based upon the free-stream unit Reynolds number and the wetted length. Measurements at the same stations relative to the corner as with configuration 10S-20 in Fig. 3 were made for configuration 15B-20. Profiles obtained at Stations A and C are shown in Fig. 4b for the same

free-stream conditions: Mach 5 and $(Re/in.)_\infty = 0.086 \times 10^6$. The change of profile shape is basically associated with the influence of the nose blunting. In both figures, the height (η) below that where the Mach number ratio equals zero is the reversed flow region. The data in Figs. 4a and b indicate that the slope of the reverse flow boundary is largest for the blunted cone, whereas the upstream extent of separation is indicated to be somewhat larger for the sharp cone.

Typical experimental results of laminar profiles measured on the hollow cylinder alone at $M_\infty = 4$ and 5 are compared with theoretical (Ref. 19) profiles for a flat plate in Fig. 5. Although the thicknesses are in close agreement, the experimental profiles are fuller or more nearly linear than theory predicts. Because probe size effects are obviously present, such limited comparisons can not be considered conclusive.

Experimental, $M_\infty = 4$, boundary-layer profiles for the hollow cylinder, 10-deg sharp cone, and 15-deg blunted cone are presented for comparison in Fig. 6. As might be expected, the non-dimensional thickness is smallest on the cone-cylinder (10S) configuration and largest on the blunt-cone cylinder (15B) although the distinction between the hollow cylinder (HC) and 15B is relatively insignificant. However, it should be recognized that for a given cylinder (centerbody) length at a given free-stream unit Reynolds number the absolute boundary-layer thickness at the end of the cylindrical section would be approximately the same for the 10S and 15B configurations because of the wetted lengths. Obviously, therefore, the hollow cylinder boundary-layer thickness is least of all. It must be pointed out that with the 10S nose, the profile parameter was essentially as shown in Fig. 6 at locations from 3 to 5R downstream of the shoulder ($\Delta x_C = 0$). However, the thickness parameter (for a given M/M_δ) was found to decrease by as much as 10 percent at locations surveyed within about 1R of the shoulder. On the other hand, the profiles shown for each configuration are typical of surveys obtained at other stations; thus, η is a satisfactory similarity parameter to generalize these results.

The boundary-layer measurements are summarized in Fig. 7 in terms of η_V, the boundary-layer thickness parameter, as a function of free-stream Mach number for the three configurations of interest. Theoretical flat-plate values to Mach 5 are included for reference. The dotted curve is also given to show that the laminar boundary-layer thickness, at least at supersonic speeds, grows approximately as the square of the free-stream Mach number.

3.5 REYNOLDS NUMBER EFFECTS ON LAMINAR FLOW SEPARATIONS

First, the influence of unit Reynolds number on the extent of separation is demonstrated in Fig. 8 for both geometry and free-stream Mach number fixed. Results obtained with configuration 10S-20 at $M_\infty = 4$ are shown in Fig. 8a for a five-fold unit Reynolds number increase. The beginning of separation, as noted in Fig. 3, clearly moves downstream for a Reynolds number increase. Thus, the extent of separation decreases with increasing Reynolds number and finally disappears at $(Re/in.)_\infty = 0.24 \times 10^6$ since transition from laminar to turbulent flow begins prior to the expected location of laminar separation. Similar trends are shown in Fig. 8b for HC-20 at $M_\infty = 3$, but the change in extent is notably less than with the sharp cone nose. Data for the 15-deg blunted cone (15B-20) in Fig. 8c also show that the extent of laminar separation upstream of the flare increases with decreasing unit Reynolds number, despite the fact that the flare pressure gradients in the region of the reattachment zone are appreciably reduced. Finally, the change in separation extent produced by a length increase at fixed unit Reynolds number and Mach number is demonstrated in Fig. 8d. These data show that the extent of separation upstream of the corner $(\xi/R)_0$ increased as a result of a Reynolds number increase. On the other hand, an opposite trend was previously demonstrated quite clearly when increasing the unit Reynolds number (see also Fig. 11). However, since it is accepted that the boundary-layer thickness is an important similarity parameter to this problem (e. g. Ref. 10), a brief consideration of its variation in relation to these seemingly conflicting data will clarify the results. Since the laminar boundary thickness can be expressed by

$$\delta = \eta_v \left[\frac{x}{(Re/in.)_\infty}\right]^{1/2} \tag{1}$$

it is obvious that the thickness decreases when increasing only the unit Reynolds number to achieve an Re_x increase, whereas δ grows when increasing the length alone to obtain increased Reynolds number. Thus, these results are unified through the realization that the upstream extent decreases when the boundary-layer thickness at separation is reduced.

Before proceeding, it is perhaps of some general interest to discuss a novel method for detecting the beginning of transition. For the flare angle considered thus far ($\theta = 20$ deg), distinct separation zones are evident with pure laminar boundary layers, whereas with turbulent flow well upstream of the flare no separation is present. Therefore, the beginning of transition may be determined for a fixed length body by noting the unit Reynolds number at which any separation zone is evident ahead of the flare. Conversely, for a variable length body, at a fixed unit Reynolds number, the location is noted to be the flare position

(length being reduced) at which any separation first appears. Typical data illustrating the above reasoning is given in Fig. 8e for the HC-20 configuration at Mach 4. The line marked "transition location" represents a conventional schlieren determination. Although smaller increments in unit Reynolds number over part of the range would have been helpful, it should be obvious that x_o reaches x_c at essentially the same conditions as indicated by the conventional method for transition location. It may also be noted that this method may be applied without flow visualization, since examination of the surface pressure distribution is an equivalent technique. In general, when transition encroaches on separation, the edge of the reversed flow region becomes curved and the length of plateau pressure region essentially shrinks to zero. At present, it is believed that this technique for locating the start of transition should be restricted to supersonic speeds ($1.5 < M_\infty < 6$), because of a lack of understanding of the separation phenomena beyond this range, particularly at hypervelocity speeds.

3.6 MACH NUMBER EFFECTS ON LAMINAR FLOW SEPARATIONS

A typical effect of Mach number on the separation extent is illustrated in Fig. 9a for the 10S-20 configuration at fixed free-stream unit Reynolds number and centerbody length. It is evident that the upstream extent grows appreciably with increased Mach number, and this trend is that usually observed in wind tunnel test programs for comparable configurations. The flare pressure distribution is shown in terms of pressure coefficient and pressure ratio to accent the appreciable dependence of the overall flare pressure rise on Mach number. Because bow-wave total pressure losses increase with Mach number, the local unit Reynolds number will be decreasing. Thus, with closed nose bodies combined effects are present which should tend to accentuate the influence of Mach number on the separation extent. A truer representation of the effect of Mach number is shown by results for the hollow cylinder in Fig. 9b. The cylinder pressures indicate small increases from Mach 2 through 4 with a more pronounced change between 4 and 5 for the beginning of the interaction as well as the plateau pressure. This result suggests that factors other than the effect of Mach number alone are involved. The pressure distribution on the frustum is worthy of notice because the pressure gradient downstream of and near to the reattachment zone is indicated to be fairly independent of Mach number. A similar effect is evident in Fig. 9a despite the large changes in the location of the reattachment zone. Some additional photographs of the separation on the small ($R = 0.5$ in.) hollow cylinder configuration are shown in Fig. 9c for $M_\infty = 3$, 5, and 8. In this instance, particularly between Mach 3 and 5, the increased extent is accompanied by a pronounced rearward movement of the reattachment zone. This is due to the fact that the plateau pressure

increases faster at small Re_{x_O} than at large values. As demonstrated in Ref. 2, the plateau pressure rise varies inversely as the fourth root of the Reynolds number at separation; thus, for small flow deflections the lift-off angle (ϕ) of the reversed flow region may be considered directly proportional to the plateau pressure rise. Since a large change in extent occurs between M_∞ = 3 and 5, a large increase in lift-off angle is also required; hence, the combined effects cause the pronounced shift of reattachment noted.

3.7 HYPERSONIC FLOW SEPARATIONS

Data obtained at Mach 8 for the 20-deg frustum with the various noses are presented in Fig. 10 for a range of Reynolds numbers. Contrary to the results in Ref. 5, there is indeed an influence of unit Reynolds number upon the extent of separation, and furthermore it is basically the same as for supersonic speeds. Negligible flow separation is indicated at maximum Reynolds number for the HC and 10S noses, because the transition process began before the corner. Of particular interest are the data for 15B-20 at minimum Reynolds number, because no change in separation location took place for a decrease in unit Reynolds number from 0.15 to 0.09 million per inch. It would appear from the flare pressure distributions, in Fig. 10b, that the probable reason for this was because the reattachment process was restricted by the flare length available. Thus, through a reduction of overall pressure rise in the reattachment zone, a compensating influence was imposed on the upstream extent of separation. Certainly, the failure to achieve a peak pressure on the flare is the most obvious difference from the HC and 10S configurations. It is, however, possible that the favorable pressure gradient along the centerbody had some influence.

3.8 CORRELATION OF FLOW SEPARATION GEOMETRY

Either for the case of turbulent flow or with laminar flow separation present, the maximum positive pressure gradient on a frustum is obviously less than theory because of the boundary layer. Therefore, if it is assumed that the pressure gradient is inversely proportional to the laminar boundary-layer thickness at the start of the frustum, a suitable non-dimensional pressure gradient expression may be written as

$$\frac{d\,(p/p_\infty)}{d\,(x/x_c)} = f\left(\frac{x}{\delta}\right)_c$$

Since it is the unfavorable pressure gradient which causes separation in the first place, and inasmuch as it has been demonstrated that the

boundary-layer thickness at the corner governs the upstream extent of the separation, a correlation of the lengths involved was tried in terms of (x/δ), which is related to free-stream conditions through Eq. (1) as

$$\frac{x}{\delta} = \frac{\sqrt{Re_x}}{\eta_v} \tag{2}$$

As an example of the data correlation, the six schlieren photographs in the Fig. 11a were analyzed to demonstrate its application and two important restrictions. Because the separation is more pronounced with small models (larger values of δ/x at a given unit Reynolds number), the 1.0-in.-diam hollow cylinder with 20-deg flare at Mach 5 was chosen. The location of separation in this case was found by an extrapolation of the edge of the reverse flow region as a straight line to the cylinder surface. This distance, x_o, the specified free-stream conditions, and Fig. 6 (η_v) were utilized to compute the non-dimensional location of separation, $(x/\delta)_o$. The non-dimensional corner location, $(x/\delta)_c$, was computed the same way, but using the distance x_c. The results in Fig. 11b show that a satisfactory correlation is realized as long as the reattachment zone is not too close to the rim of the flare. The separation position in photographs 1 and 2 is seen also to remain fixed under such conditions, as noted previously at hypersonic speeds (in Fig. 10a). The lift-off angle, ϕ, of the reverse flow boundary, is plotted in Fig. 11c versus the relative extent of separation, ξ_o/x_c, to illustrate the restraint on the geometry of the reverse flow zone when separation approaches a forward physical limit.

Most of the experimental results for the HC-20 configuration have been analyzed to provide the correlation of separation extent, for a wide range of conditions, as indicated in Fig. 12. Numerous points have been excluded from this figure in order to clarify the apparent dependence of the conditions near separation on the conditions at the start of the flare. As indicated by the examples in Fig. 11, those points for which either rim restraint or lip restraint was present were excluded. In addition, an attempt was made to exclude the data for which the plateau pressure was not fully established prior to the frustum, and based upon the general observation that the lift-off boundary is always curved in such cases, those data for the small model were excluded also. As noted previously, data of this kind are caused by the closeness of transition to separation, and the extent of flow separation was found to be always less than that present for the fully developed plateau. Thus, the extent of flow separation is never more than that indicated by the correlation, regardless of the proximity of transition to reattachment.

Considerably more data are included in this correlation curve than in Ref. 20, and so the fairing has been shifted slightly to be more

representative. It is obvious, however, that an appreciable deviation from the data fairing is present. Whether this represents unaccounted-for functional variations is not known, but it is clear from the experience of having analyzed the extensive experimental results that some margin of choice in locating x_o is inevitably present. Within the range of $40 < (x/\delta)_c < 150$, it appears that ±5 is representative of the deviation in $(x/\delta)_o$. An approximate analysis indicates that this deviation represents a variation in x_o ranging from about 12 to 6 percent of the cylinder length, x_c, respectively, for the above cited range in $(x/\delta)_c$. For test conditions where $(x/\delta)_c < 40$, a non-linear variation of $(x/\delta)_o$ is indicated and should be expected, since in the limit $(x/\delta)_o$ must approach zero as $(x/\delta)_c$ tends to zero. It is within this regime that most hypersonic and hypervelocity testing is done, and so it should be apparent from the data in Fig. 12a that a suitable definition of a correlation curve is expected to be most difficult. No doubt, because of the significant viscous effects usually present in this regime, a substantially different effect of the boundary layer is to be expected.

An important and large discrepancy is indicated by the two points shown in Fig. 12a for Mach 6. Because the ambient conditions were far below the equilibrium saturation level for air, air liquefaction (about 3 percent) of free-stream flow is known to have occurred. Thus, this isolated difference is attributed to an unexpectedly pronounced influence of air liquefaction on laminar separation.

For the flare angle being considered (θ = 20 deg), it was found that the flow separation was incapable of propagating past expansion corners of at least 10 deg; therefore, for better comparison with the open nose data, both of the coordinates of Fig. 12a were changed for a correlation of the separation extent with configurations 10S-20 and 15B-20. The coordinates in Figs. 12b and c thus measure the separation and flare locations relative to the shoulder position, in terms of $(x/\delta)_s$. Within the probable tolerance of locating the beginning of separation, it appears that a comparable correlation is realized for the closed nose configurations, as with the hollow cylinder in Fig. 12a. That is, the difference in $(x/\delta)_c - (x/\delta)_o$ is on the order of twenty for all configurations in the range of $\left[(x/\delta)_c - (x/\delta)_s\right] < 40$. The Mach 6 data have been retained in Fig. 12c, since air liquefaction did not increase the separation extent as with the hollow cylinder. Because condensed flows tend to disappear in crossing strong shock waves, it would appear that with the 15B-20 configuration liquefaction was locally absent.

3.9 INFLUENCE OF FRUSTUM GEOMETRY

Within a very broad range of test conditions, the extent of the reverse flow region upstream of a 20-deg flare has been demonstrated to be essentially a constant, $\xi(\theta)$. That is, it may be said that

$$\left(\frac{x}{\delta}\right)_c - \left(\frac{x}{\delta}\right)_o = \xi(\theta) \tag{3}$$

is a constant, realizing that important model geometry limits may exist under certain conditions, and that boundary-layer transition also affects the constant whenever a well-developed plateau pressure does not occur. In general, as long as separation or reattachment does not approach closely either the shoulder or the rim of the model, the correlation constant is valid for a given frustum geometry. Data obtained with different flare angles are presented in Fig. 13 to show the variation in separation extent associated with compression surfaces. Two-dimensional (flap) data are also included in this figure to show that there is no significant difference between flat plate and axisymmetric laminar flow separations. It will be noted that the curve faired through the data ignores the data (HC) of Ref. 13 for $\theta > 20$ deg. The data of Pate in Figs. 6 and 7 of Ref. 6 indicate quite clearly, for $\theta = 30$ deg, that when transition occurs well upstream of the corner, but downstream of separation, that the extent parameter is appreciably greater (about 38) than that for a pure laminar separation. As noted previously in Section 3.5, the magnitude of $\xi(\theta)$ decreases as transition approaches separation closely, when the flare angle is less than that required to induce turbulent flow separation upstream of the corner. And since the extent of pure turbulent flow separation is less than for pure laminar separation, it follows that the extent parameter, $\xi(\theta)$, is the greatest for truly transitional flow separations. In other words, when the flow deflection is large enough to separate turbulent flow, a substantial region of pure laminar separation may exist upstream of the turbulent separation with the extent of the combined separations being greater than either type alone. Since the results of Lee (Ref. 13) show that transition could, in fact, occur ahead of the flare corner, it is reasoned that his data for $\theta > 20$ are truly transitional and should be ignored in this case. Based upon these considerations, it is reasoned that for flow deflections of greater than 25 deg (approximately), the relative extent of separation may increase with increasing Reynolds number when transition approaches reattachment. Conversely, for smaller flare angles the relative extent of separation always decreases when increasing the Reynolds number, regardless of the location of transition.

3.10 PLATEAU PRESSURE CORRELATIONS

The non-dimensional pressure rise to the plateau level for laminar flow separation is presented in Fig. 14 as a function of the separation

Reynolds number, Re_{x_o}, for the three nose configurations. Since more extensive data were obtained with the hollow cylinder nose, it is possible to show results for different centerbody lengths at a given Mach number. Only those data are presented for which a well-developed plateau existed and for which there was no question of geometric restraints. Despite these restrictions, it is apparent by the scatter in the results that there is a considerable tolerance involved in this correlation also.

The effects of Mach number on the plateau correlation parameter, $C_{p_p} Re_{x_o}^{1/4}$, and a comparison with various two-dimensional results are shown in Fig. 15. These data show that the correlation is the same for a flat plate as for a cylinder. However, as would be expected because of skin friction differences, the results in Figs. 14b and c may be used to show that axisymmetric closed nose configurations do not, in general, yield the same plateau correlation as the hollow cylinder. The correlation of Erdos and Pallone (Ref. 10) has been extended, as in Ref. 5, to Mach 16 to show the good agreement beyond the hypersonic speed range. A calculation of $C_{p_p} Re_{x_o}^{1/4}$ (based on Van Driest's results in Ref. 21 as applied by Erdos and Pallone) was made for Mach 20 to illustrate the effect of wall cooling upon the plateau pressure at hypervelocity speeds. It was found that for $T_w/T_\infty = 0.25$ the value of $C_{p_p} Re_{x_o}^{1/4}$ is about 17 percent greater than that expected for the insulated wall case. This effect is less than experimental scatter shown at Mach 13.

3.11 INCIPIENT SEPARATION

The conditions at which flow separation first appears may be termed as incipient flow separation conditions. Definition of the general conditions governing the onset of separation is important and has been investigated rather broadly by Kuehn (see, particularly, Ref. 14). However, from the present research, it should be obvious that no sharp distinction really exists between attached and separated flows when the separation is small relative to the ramp or flare. Although the selection of suitable criteria to define the onset of separation is necessarily somewhat arbitrary, the ultimate distinction to be made is between the existence of significant and inconsequential reverse flow regions.

Using surface pressure distributions to detect the onset of a pressure plateau, Kuehn was able to conclude that the tendency of flow to separate decreases with either decreasing Reynolds number or increasing Mach number. Such tendencies are contrary to the results of the present research, particularly the finding herein that the relative extent of

separation increases with decreased Reynolds number. Besides the fact that the flare angles used here were appreciably larger than those used by Kuehn, his results indicate that relatively small Reynolds numbers would be required to eliminate separation on the configurations discussed in this report. In fact, it can be shown that these would be conditions below the deviation point of the extent correlation, $\left[(x/\delta)_C - (x/\delta)_S\right] \leq 40$, and thus the similarity of such flow separation to the usual flow model is believed to be considerably different. Since this flow regime is characterized by the absence of well-defined reverse regions, it appears, therefore, that Kuehn's incipient separation boundaries could possibly be considered as defining the conditions for a coupling between the separation and reattachment regions. That is, a free-interaction at separation may no longer exist.

For the range of conditions over which the extent correlation was achieved, one may examine the variation of the relative extent of separation with the parameter Re_{δ_o}, since this is the parameter Kuehn used to correlate his results. From Eq. (2), Re_{δ_o} may be defined

$$Re_{\delta_o} = \frac{Re_{x_o}}{(x/\delta)_o} \equiv \eta_v \sqrt{Re_{x_o}} \equiv \eta_v \sqrt{Re_{x_c}} \left(\frac{x_o}{x_c}\right)^{1/2} \tag{4}$$

and since $\xi_o = x_C - x_O$, the relative extent of separation is given as

$$\frac{\xi_o}{x_c} = 1 - \frac{Re^2_{\delta_o}}{\eta_v^2 \, Re_{x_c}} \tag{5}$$

It is evident, based upon the above expression, that the relative extent of separation for fixed length, x_C, and for constant Re_{δ_O} depends upon the unit Reynolds number as well as the Mach number through parameter η_V. For ξ_O/x_C to decrease at constant Re_{δ_O}, the unit Reynolds number must decrease faster than the term $\eta_V{}^2$ increases, otherwise there would be no decrease in separation extent as implied by Kuehn's results.

4.0 CONCLUSIONS

The principal finding of this experimental research is that the extent of the reverse flow region upstream of a flare (frustum) is essentially a function of the wetted length to the corner, in terms of the laminar boundary thickness there. For a wide range of conditions, it is shown that the difference in the ratio of x/δ at the corner and at the beginning of interaction is effectively a constant for a given geometry and that this constant increases with flare angle. In particular, the relative extent

of the separation increases when decreasing either unit Reynolds number or centerbody length, and Mach number increase produces an increased length of reverse flow. There is no practical difference between the separation extent for two-dimensional and axisymmetric configurations. As the hypervelocity or low density regimes are approached, $(x/\delta)_c \ll 40$, this correlation of separation extent is no longer valid. More research is required in this area.

For flare (or flap) angles of less than approximately 25 deg, the proximity of transition to the reattachment region has a negligible effect on the variation of the relative extent of flow separation with Reynolds number, as long as a well-developed plateau pressure region exists. Whenever the rise to the plateau and the rise at reattachment is blended together without a constant pressure region in between, the extent of separation will be less than that indicated by the correlation. This latter condition is considered to be more strictly representative of transitional separations, whereas the former should be classified as purely laminar separations. For $\theta > 25$ deg, a significantly different effect on the extent is indicated whenever transition occurs in the reattachment zone. That is, the relative extent of flow separation may be greater than for a pure laminar separation.

REFERENCES

1. Gadd, G. E., Holder, D. W., and Regan, J. D. "An Experimental Investigation of the Interaction between Shock Waves and Boundary Layers." Proceedings of the Royal Society of London, Series A, Vol. 226, 1954, pp. 227-253.

2. Chapman, D. R., Kuehn, D. M., and Larson, H. K. "Investigation of Separated Flows in Supersonic and Subsonic Streams with Emphasis on the Effect of Transition." NACA Report 1356, 1958.

3. Hakkinen, R. J., Greber, I., Trilling, L., and Abarbanel, S. S. "The Interaction of an Oblique Shock Wave with a Laminar Boundary Layer." NASA TM 2-18-59W, March 1959.

4. Sterrett, J. R. and Emery, J. C. "Experimental Separation Studies for Two-Dimensional Wedges and Curved Surfaces at Mach Numbers of 4.8 to 6.2." NASA TN D-1014, February 1962.

5. Miller, D. S., Hijman, R., and Childs, M. E. "Mach 8 to 22 Studies of Flow Separations Due to Deflected Control Surfaces." AIAA Journal, Vol. 2, No. 2, February 1964.

6. Pate, S. R. "Investigation of Flow Separation on a Two-Dimensional Flat Plate Having a Variable-Span Trailing Edge Flap at M_∞ = 3 and 5." AEDC-TDR-64-14 (AD 432831), March 1964.

7. Crocco, L. and Lees, L. "A Mixing Theory for the Interaction between Dissipative Flows and Nearly Isentropic Streams." Journal of Aeronautical Sciences, Vol. 19, No. 10, October 1952.

8. Gadd, G. E. "Interactions between Wholly Laminar and Wholly Turbulent Boundary Layers and Shock Waves Strong Enough to Cause Separation." Journal of Aeronautical Sciences, Vol. 20, No. 11, November 1953.

9. Glick, H. S. "Modified Crocco-Lees Mixing Theory for Supersonic Separated and Reattaching Flows." Journal of the Aerospace Sciences, Vol. 29, No. 10, October 1962.

10. Erdos, J. and Pallone, A. "Shock-Boundary Layer Interaction and Flow Separation." AVCO RAD TR 61-23, August 1961.

11. Abbott, D. E., Holt, M., and Nielsen, J. N. "Investigation of Hypersonic Flow Separation and Its Effects on Aerodynamic Control Characteristics." ASD-TDR-62-963, November 1962.

12. Cooke, J. C. "Separated Supersonic Flow." RAE Tech Note Aero 2879, March 1963.

13. Lee, J. D. "The Influence of High Adverse Pressure Gradients on Boundary Layers in Supersonic Flow." UTIA Report 21, October 1952.

14. Kuehn, D. M. "Laminar Boundary Layer Separation Induced by Flares on Cylinders at Zero Angle of Attack." NASA Technical Report R-146, 1962.

15. Ferguson, H. and Schaefer, J. W. "Heat Transfer and Pressure Distribution on Cone-Cylinder-Flare Configuration with Boundary Layer Separation." NASA TN D-1436, October 1962.

16. Lees, L. and Reeves, B. L. "Supersonic Separated and Reattaching Laminar Flows: I. General Theory and Application to Adiabatic Boundary Layer-Shock Wave Interactions." Firestone Flight Sciences Laboratory, California Institute of Technology, Tech Report 3, October 1963.

17. Test Facilities Handbook (5th Edition). "von Kármán Gas Dynamics Facility, Vol. 4." Arnold Engineering Development Center, July 1963.

18. Faye-Peterson, R. "Theoretical Aerodynamic Studies of Missiles with Flared Skirts in Supersonic Upstream Flow." IAS, SMF Fund Paper FF-31, January 22-24, 1962.

19. Mack, L. M. "Calculation of the Laminar Boundary Layer on an Insulated Flat Plate by the Klunker-McLean Method." JPL Progress Report 20-352, July 1958.

20. Gray, J. D. "A Correlation of Axisymmetric Laminar Flow Separation Characteristics." AIAA Paper No. 64-475, June 1964.

21. Van Driest, E. R. "Investigation of Laminar Boundary Layer in Compressible Fluids Using the Crocco Method." NACA TN 2597, January 1952.

TABLE 1

TESTING SUMMARY

Configuration	M_∞	x_c, in.	Re/in. x 10^{-6}	R, in.	Data* S	S/G	P	BL
HC-10	4, 5, 6	7-20	0.10-0.60	3.5	x	-	x	-
" -15	4, 5	5-20	0.07-0.55	"	x	-	x	-
-20	2, 3	7-21	0.06-0.50	"	x	-	x	-
" "	4, 5, 6	7-21	0.04-0.50	"	x	-	x	x
" "	3, 4, 5	0.5-4	0.04-0.35	0.5	x	-	-	-
" "	8	14, 24	0.05-0.30	3.5	-	x	x	-
" "	8	0.5-4	0.15-0.50	0.5	-	x	-	-
10S-15	3, 4	5-20	0.04-0.45	3.5	x	-	x	-
" -20	2, 3	7-21	0.06-0.45	"	x	-	x	
" "	4, 5, 6	7-21	0.05-0.55	"	x	-	x	x
" "	8	14, 24	0.05-0.30	"	-	x	x	-
15B-15	2, 3, 4, 5	6-20	0.04-0.55	3.5	x	-	x	-
" -20	2, 3	7-21	0.05-0.43	"	x	-	x	-
" "	4, 5, 6	7-21	0.04-0.55	"	x	-	x	x
" "	8	14, 24	0.05-0.30	"	-	x	x	-
HEMI-	4, 5, 6	21	0.04-0.43	"	x	-	-	x

*NOTE: S = Schlieren
S/G = Shadowgraph
P = Surface pressures
BL = Boundary-layer profiles

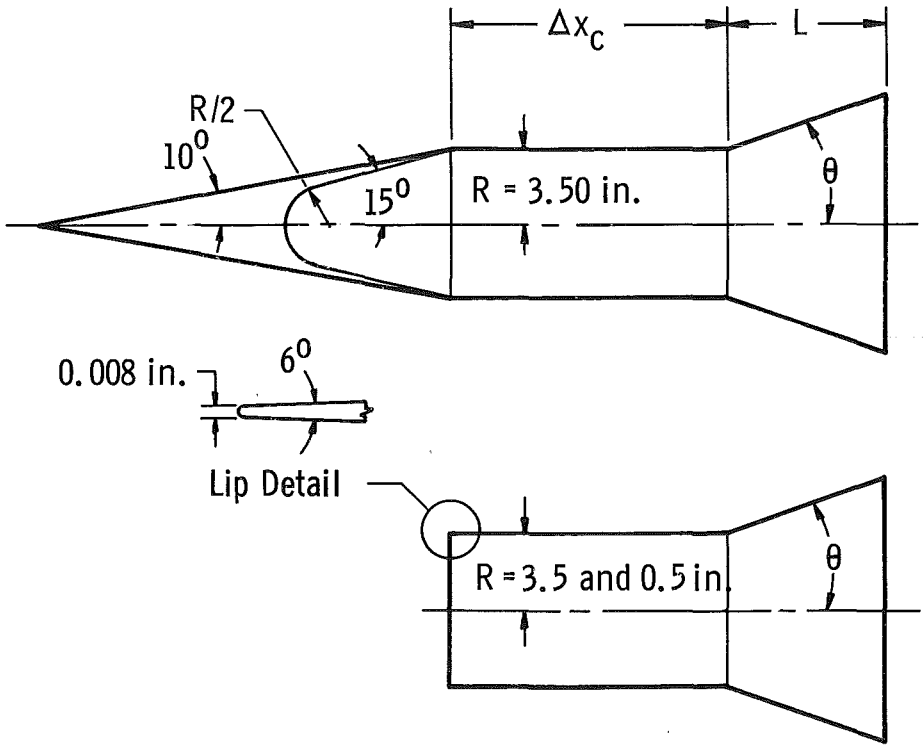

FLARES

θ, deg	L
10	2R
15	4R
20	2R

104366

a. Geometric Details

Fig. 1 Model Configurations

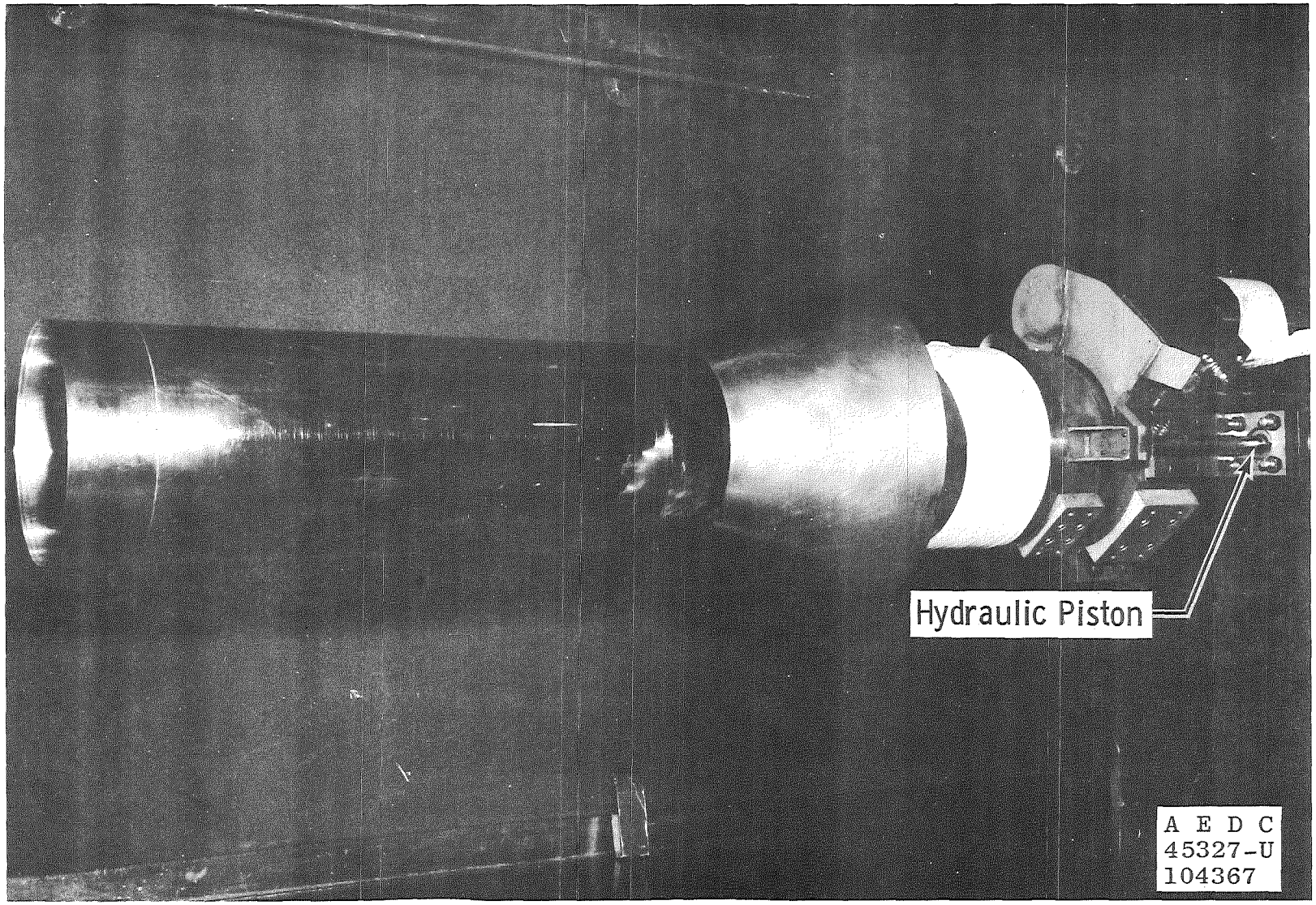

b. Typical Installation of Hollow Cylinder in Supersonic Wind Tunnel

Fig. 1 Concluded

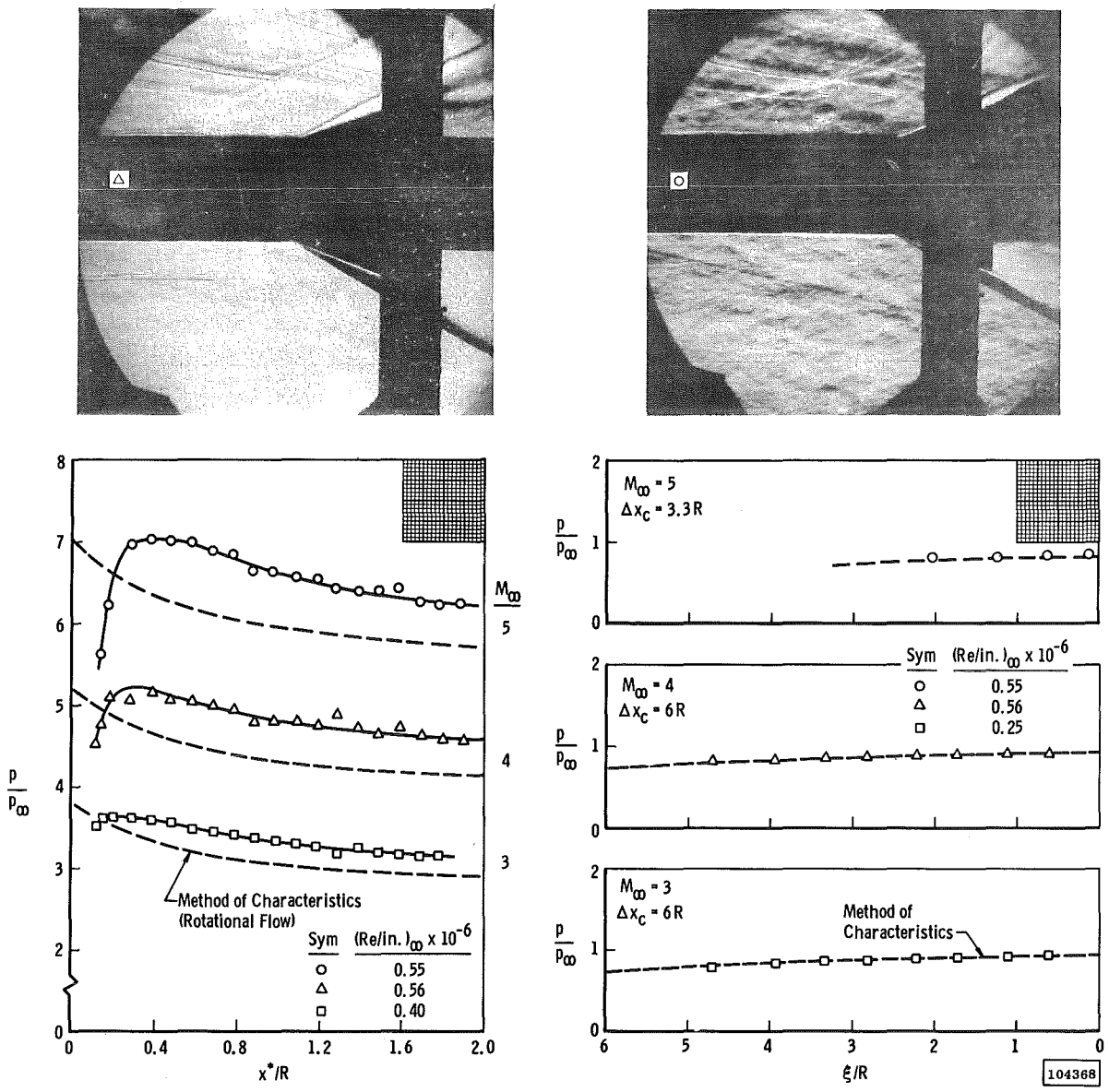

a. Frustum, HC-20 Configuration, M_∞ = 3, 4, and 5

b. Centerbody, 10S-20 Configuration, M_∞ = 3, 4, and 5

Fig. 2 Typical Pressure Distributions with Negligible Flow Separation

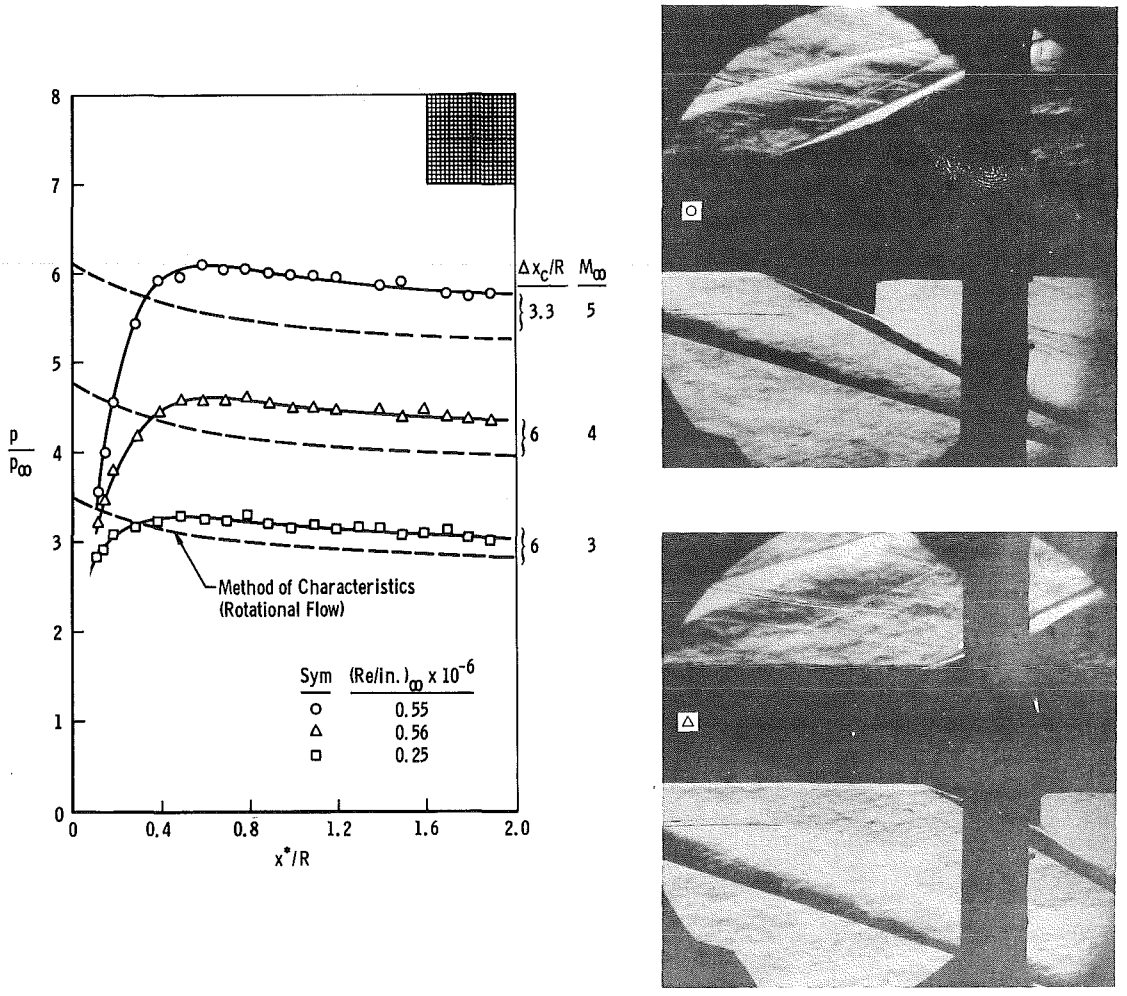

c. Frustum, 10S-20 Configuration, M_∞ = 3, 4, and 5

104369

Fig. 2 Continued

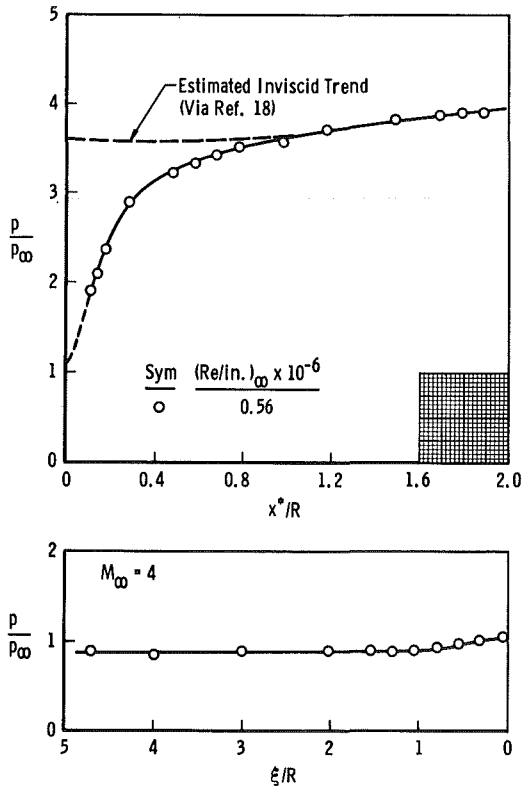

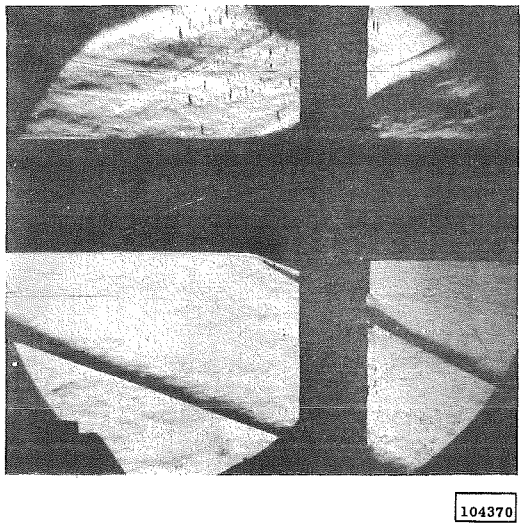

104370

d. Centerbody and Frustum, 15B-20 Configuration, $M_\infty = 4$

Fig. 2 Concluded

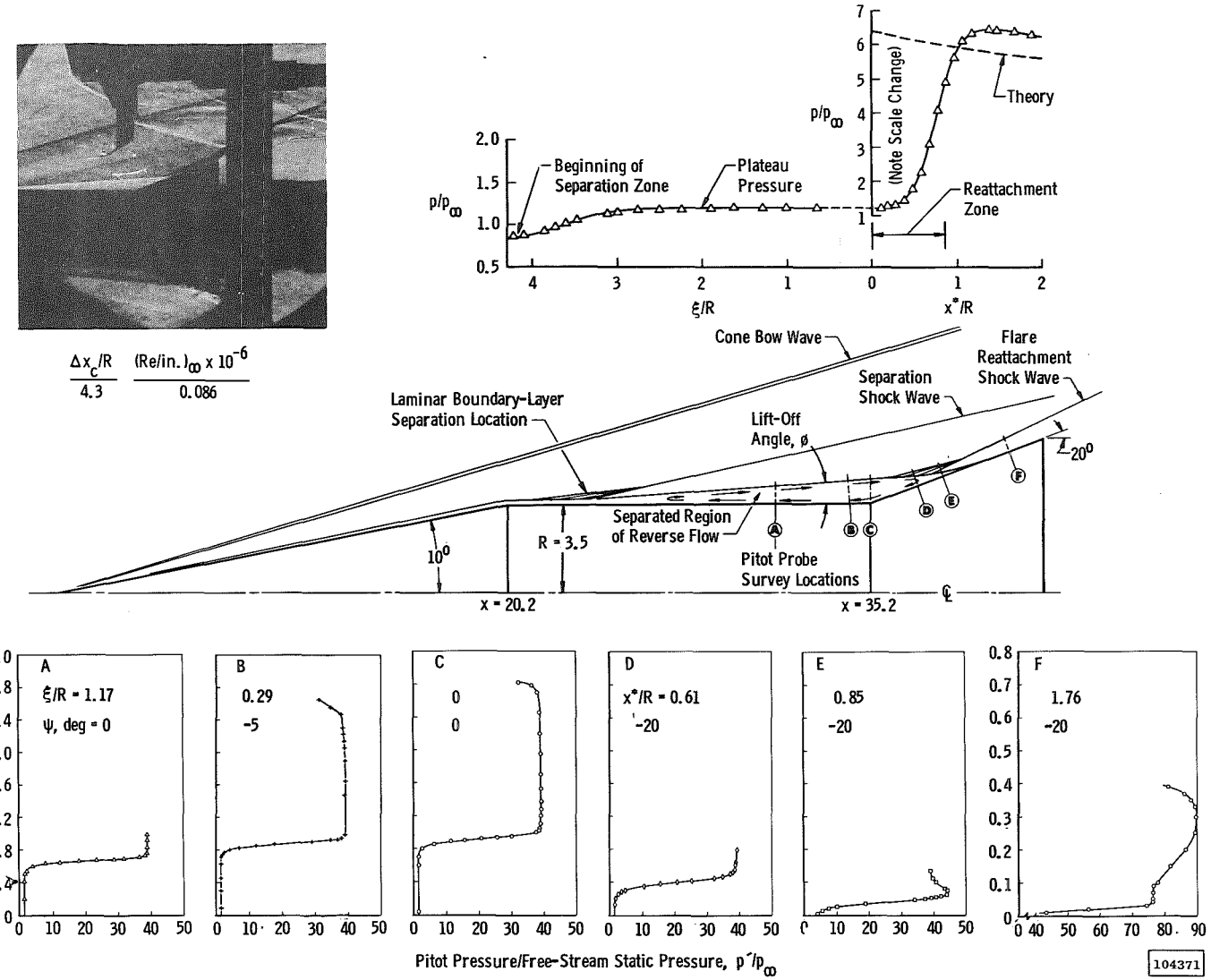

Fig. 3 General Characteristics of Shock-Induced Laminar Flow Separation at Mach 5, Configuration 10S-20

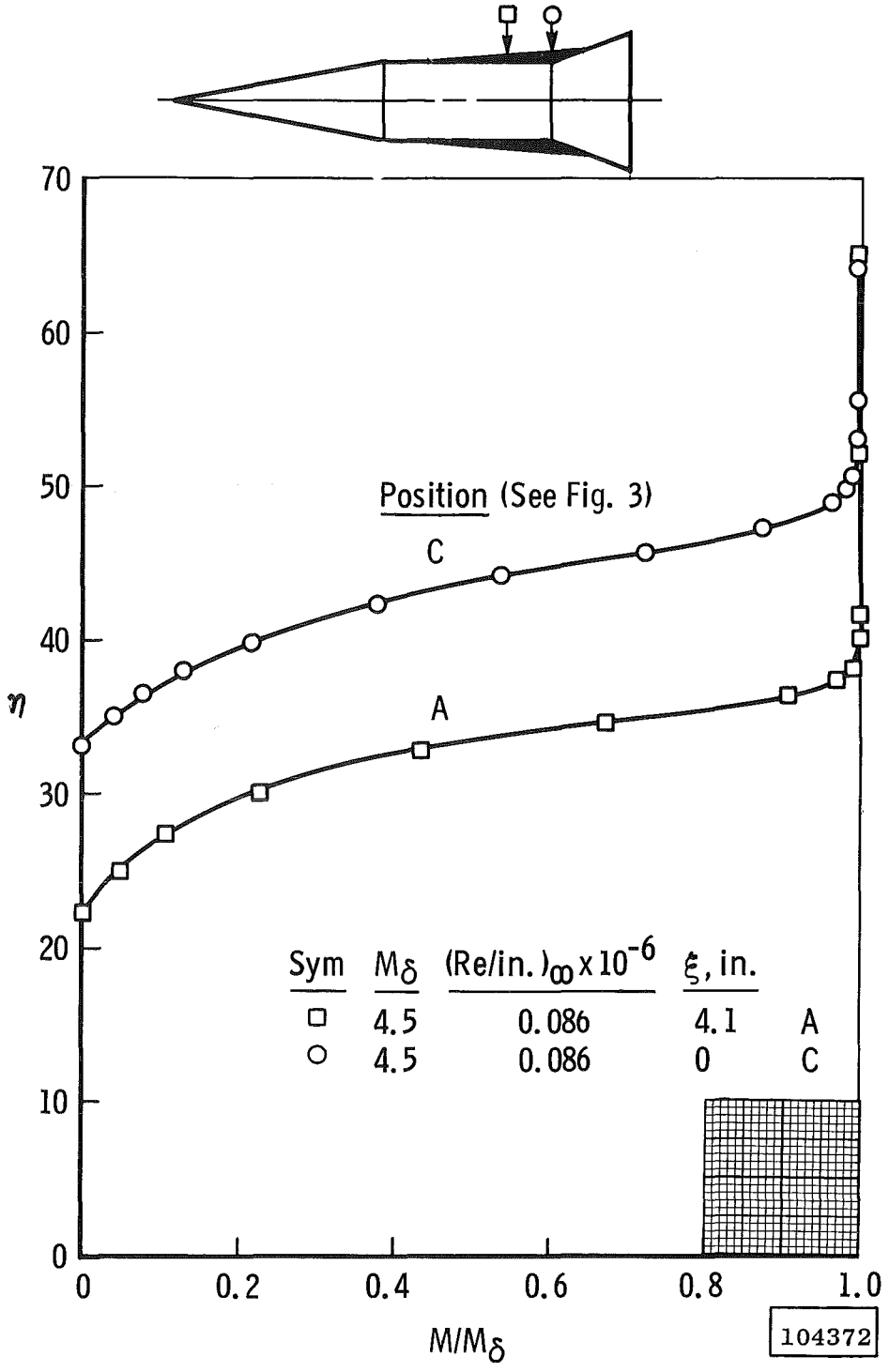

a. Configuration 10S-20

Fig. 4 Boundary-Layer Profiles above Reverse Flow Region at Mach 5

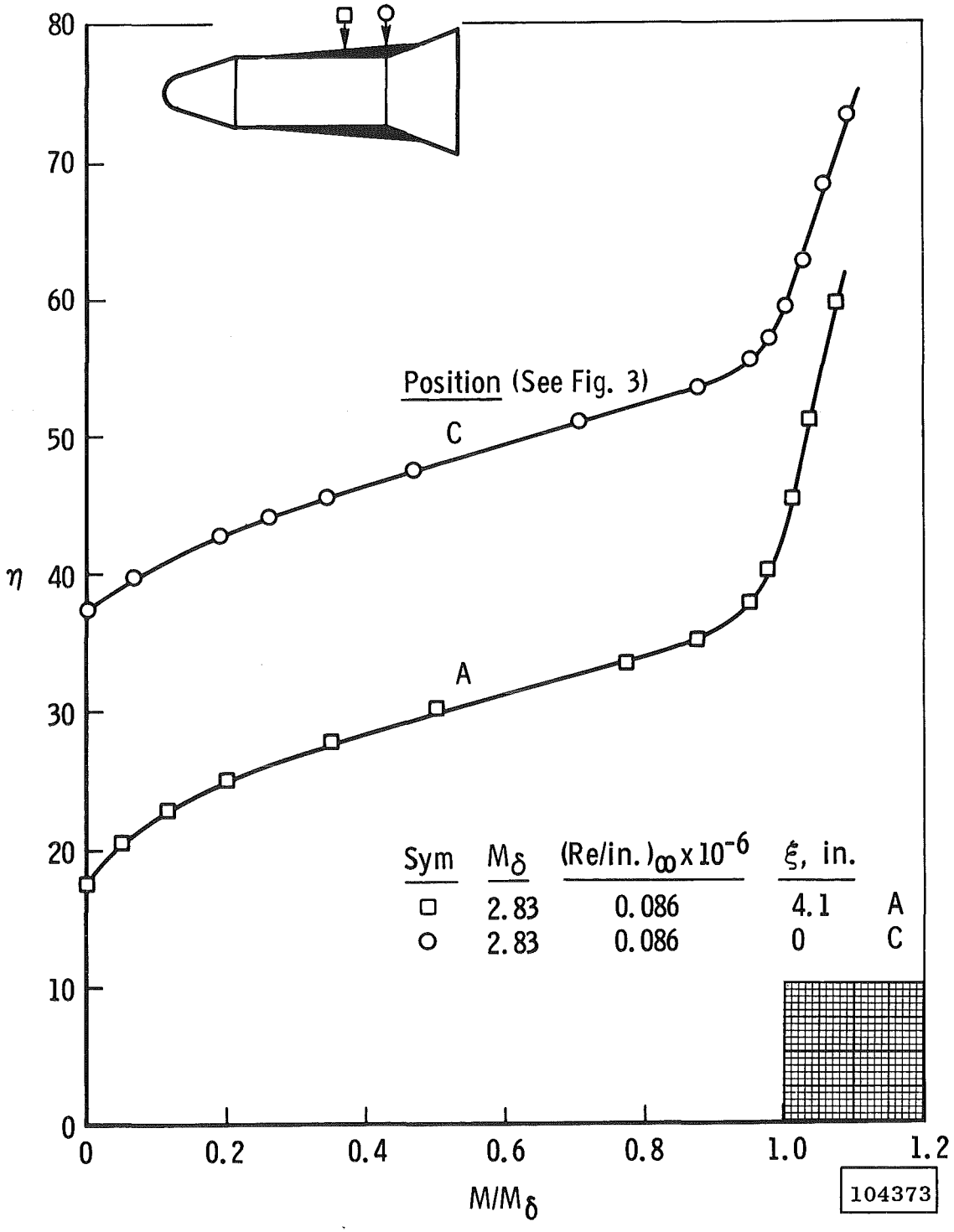

b. Configuration 15B-20

Fig. 4 Concluded

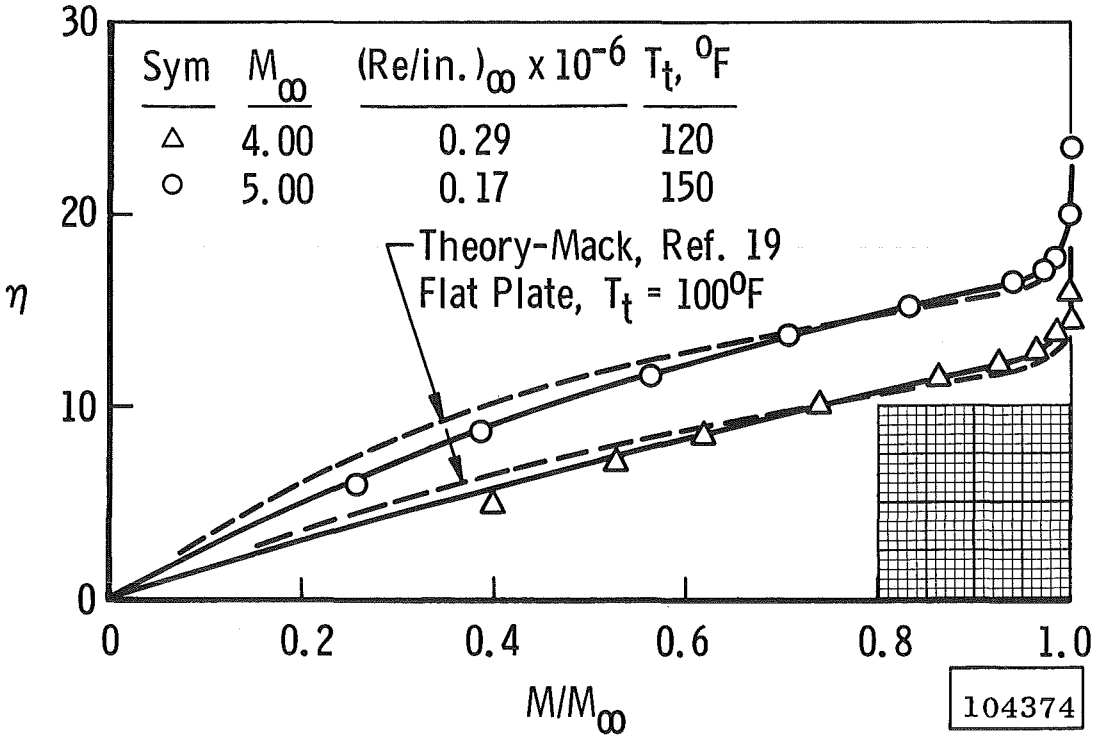

Fig. 5 Laminar Boundary-Layer Profiles on Hollow Cylinder at Mach 4 and 5

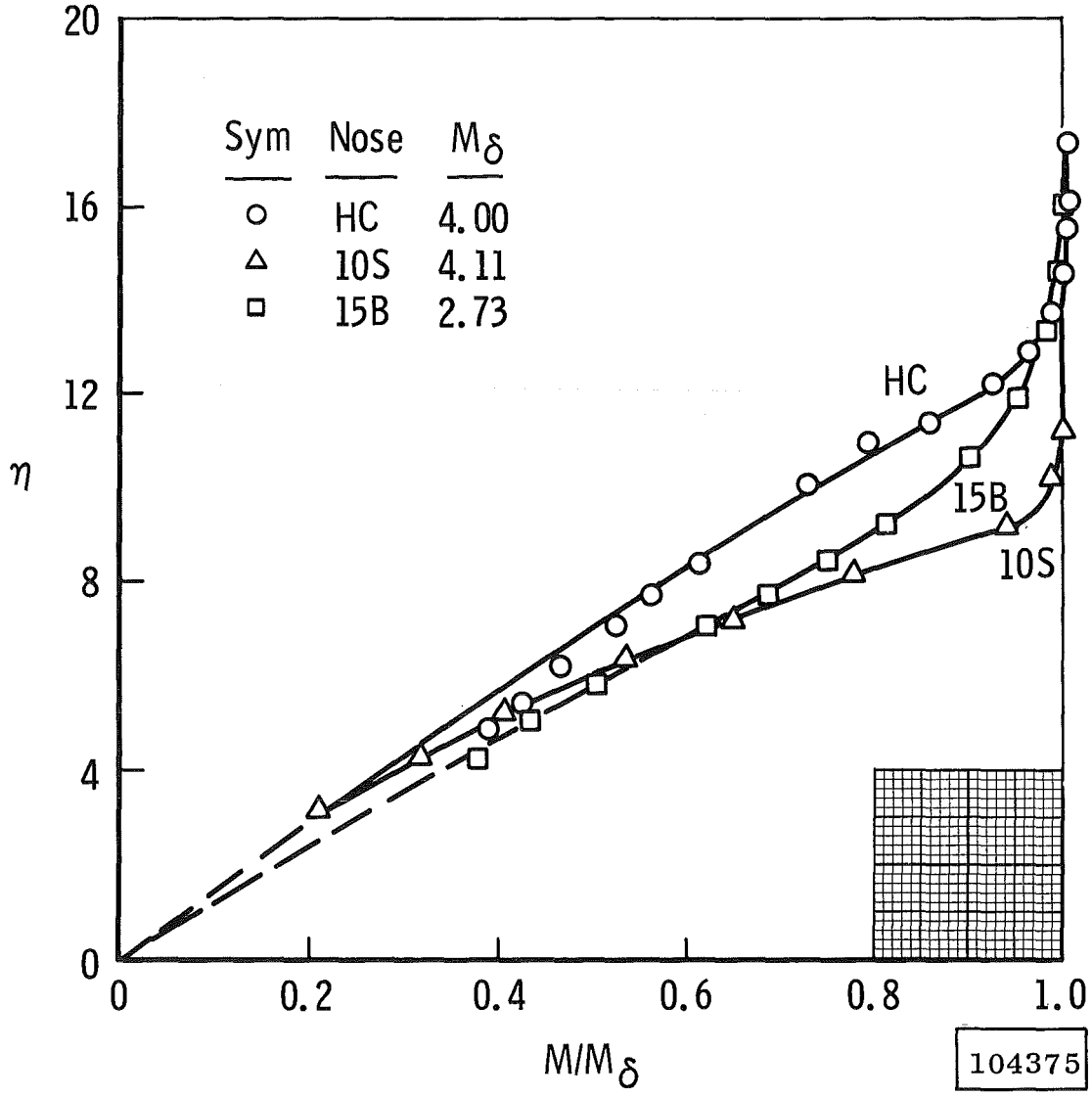

Fig. 6 Comparison of Laminar Profiles with 10-deg Sharp Cone, 15-deg Blunt Cone, and Open Noses at Mach 4

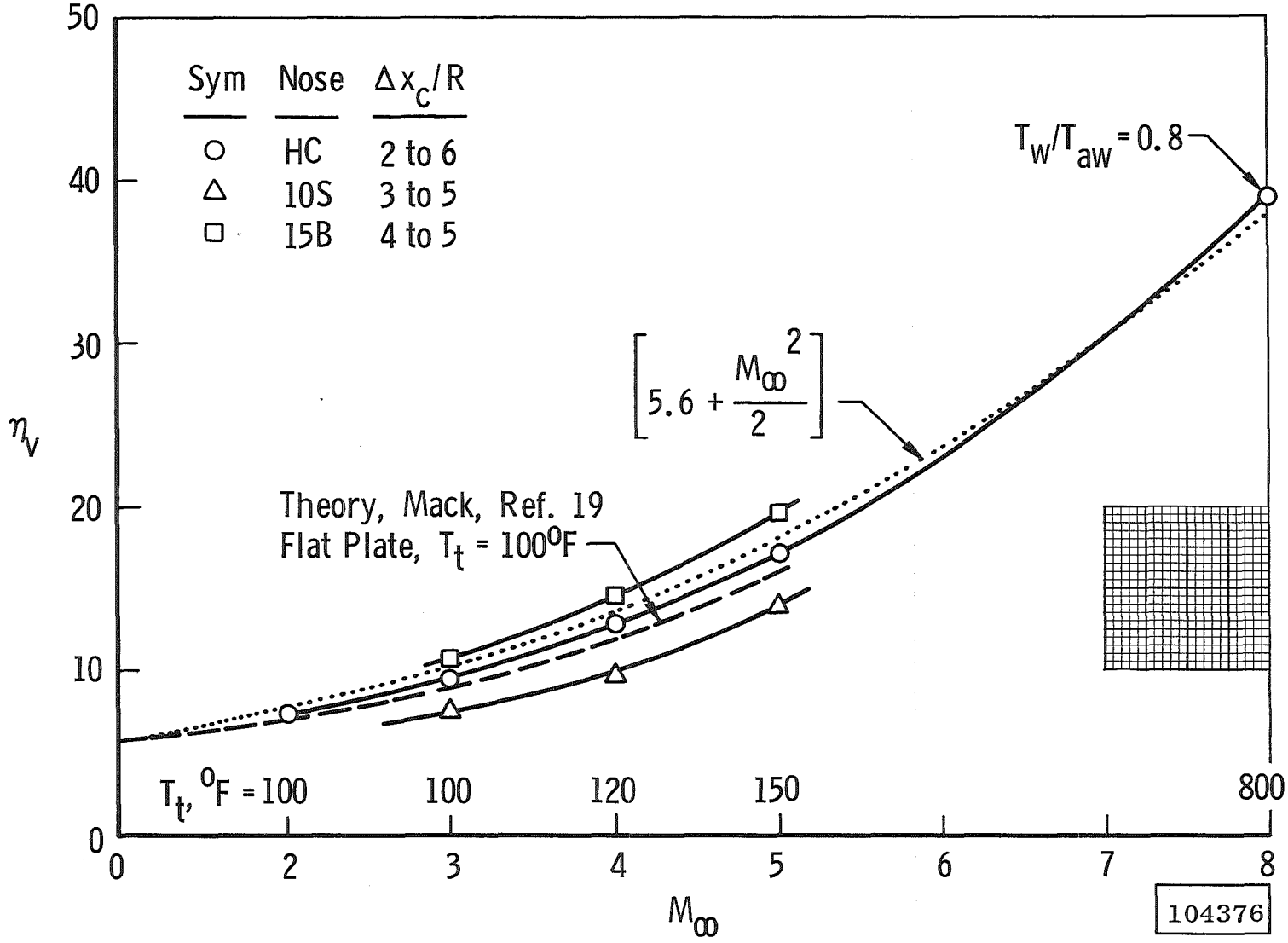

Fig. 7 Variation of Laminar Boundary-Layer Thickness Parameter with Mach Number for Several Axisymmetric Bodies

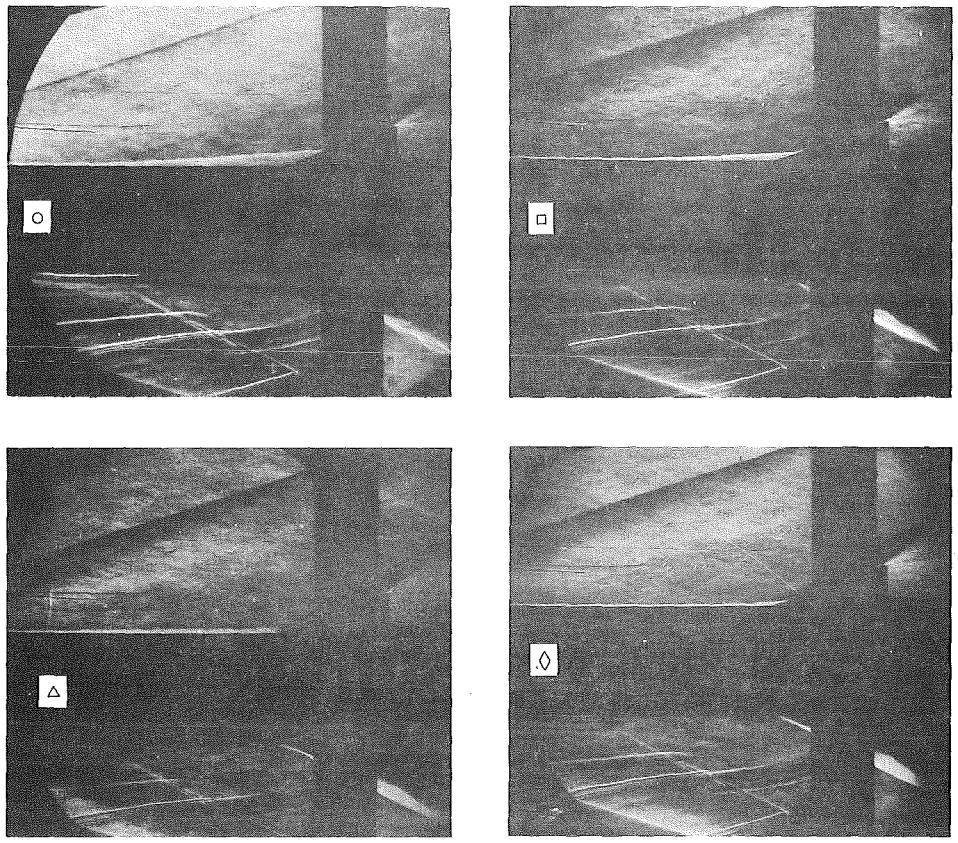

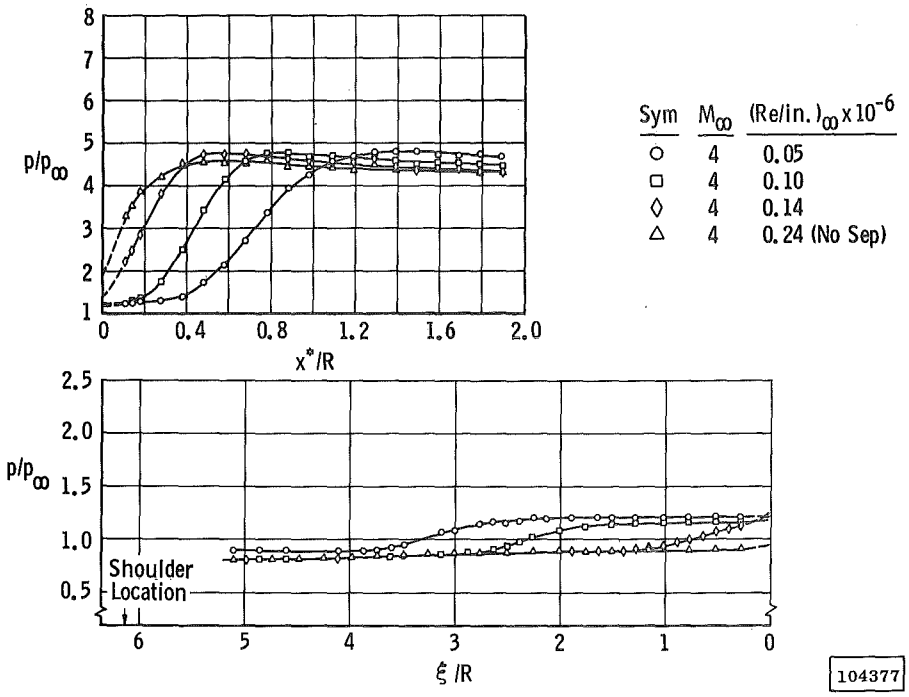

a. 10-deg Sharp Cone, $M_\infty = 4$, $\Delta x_c \approx 6.16R$

Fig. 8 Effect of Reynolds Number on Extent of Laminar Separation Induced by a 20-deg Frustum, R = 3.5 in.

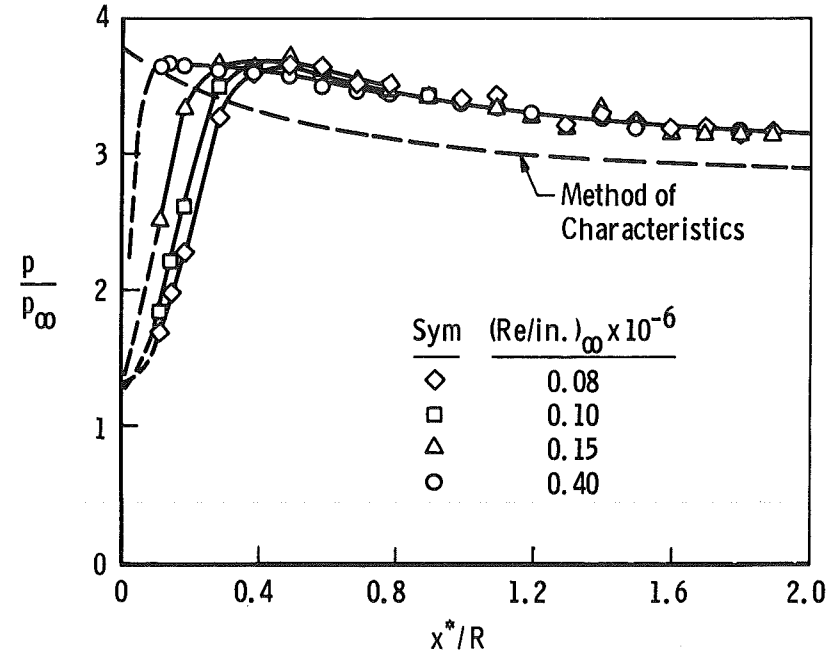

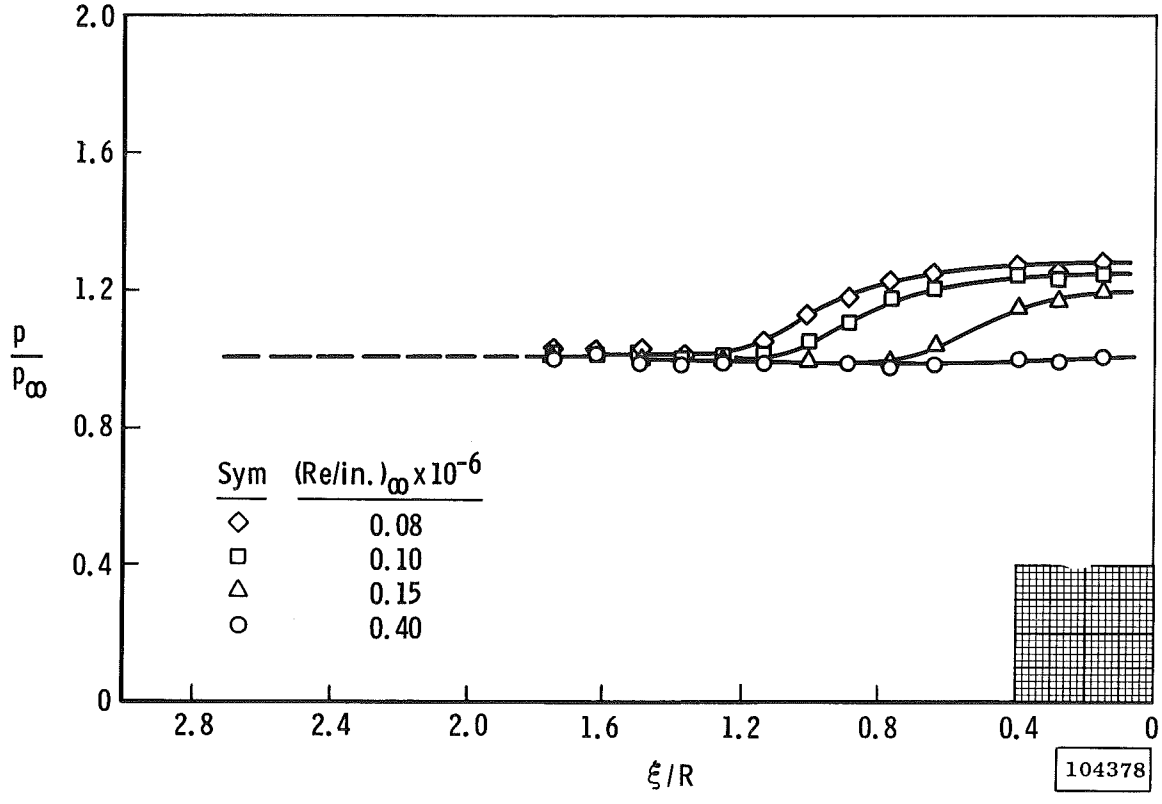

b. Hollow Cylinder, $M_\infty = 3$, $x_c = 3.0R$

Fig. 8 Continued

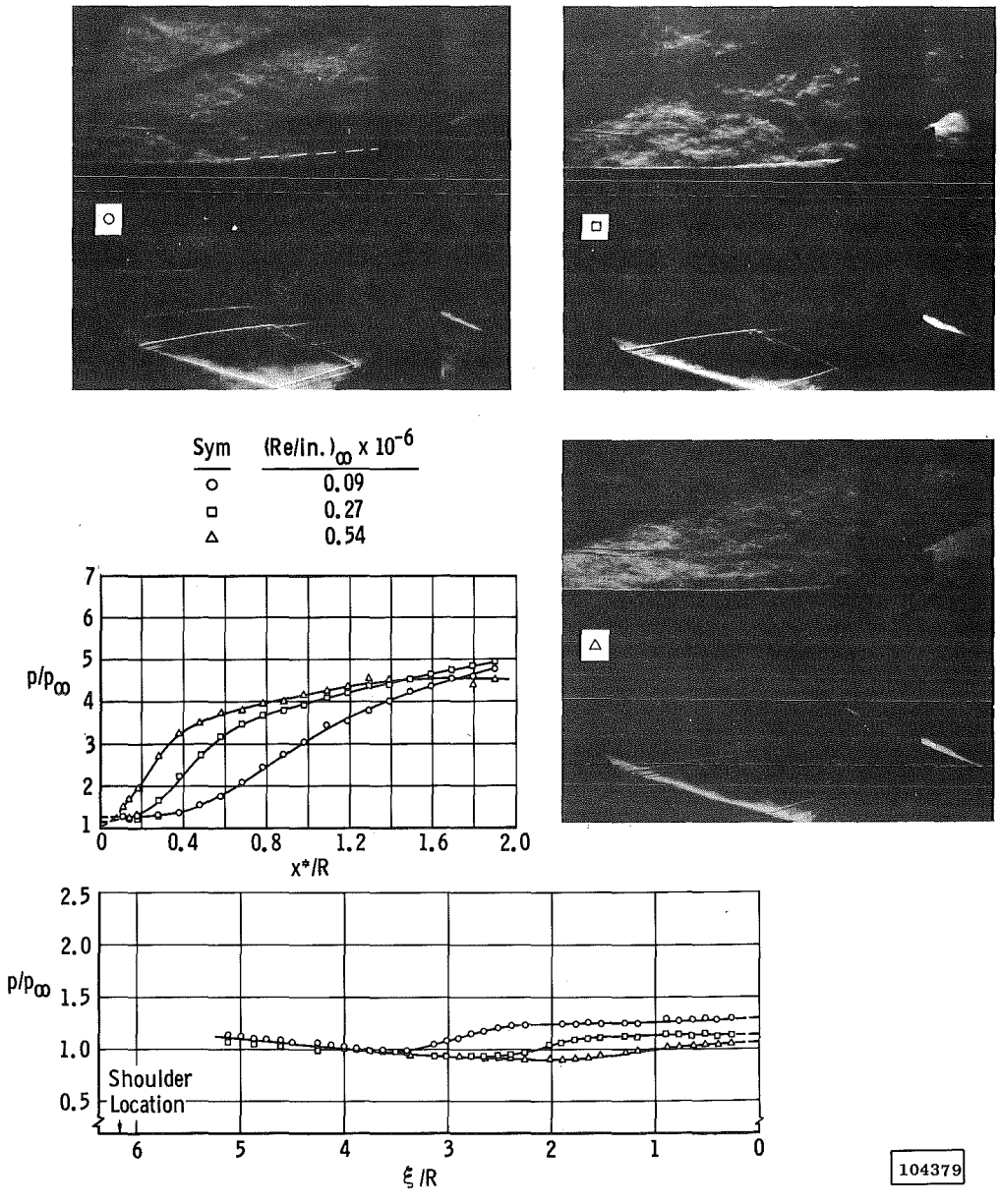

c. 15-deg Blunt Cone, $M_\infty = 5$, $\Delta x_c = 6.16R$

Fig. 8 Continued

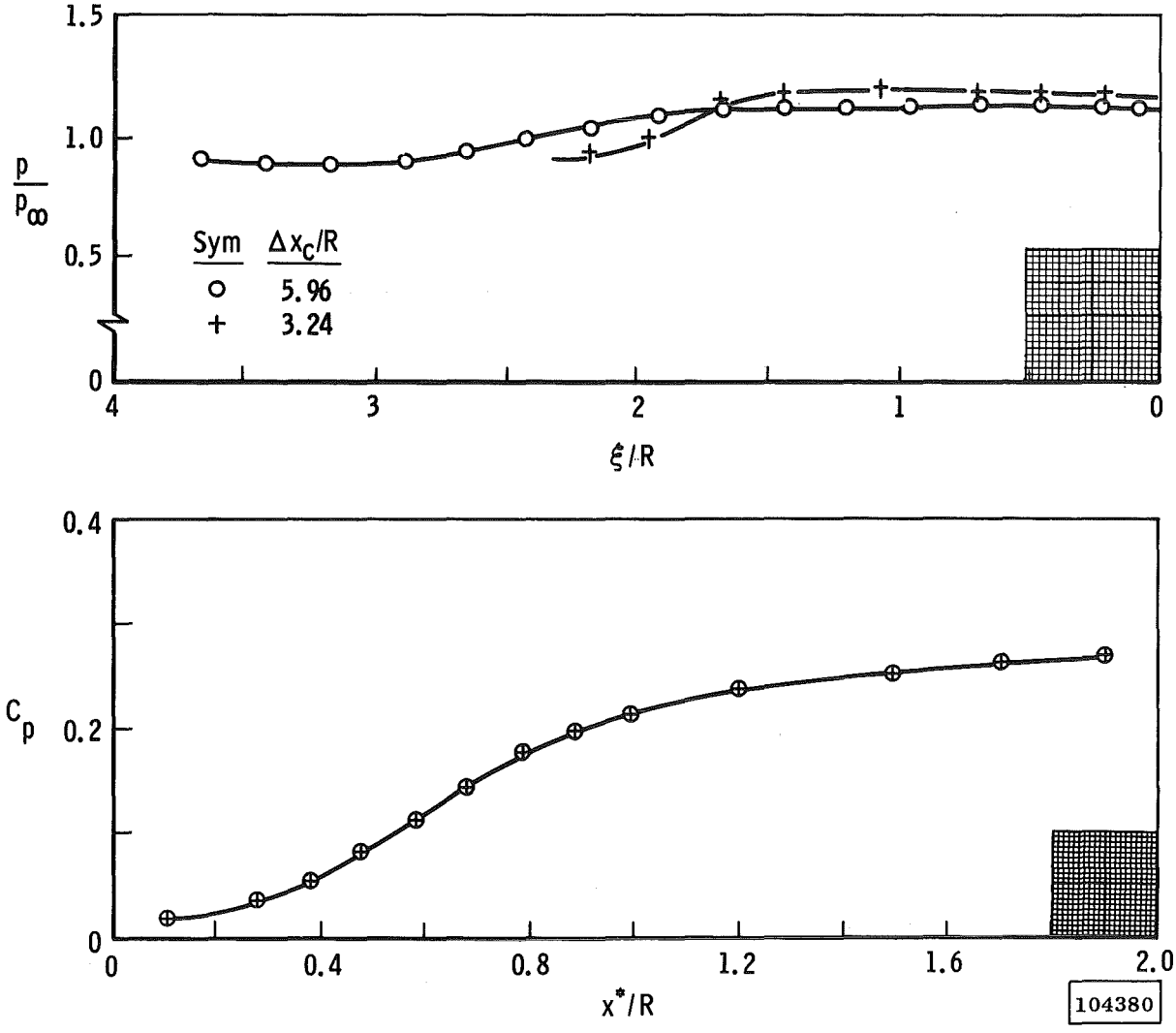

d. 15-deg Blunt Cone, $M_\infty = 4$, $(Re/in.)_\infty = 0.07 \times 10^6$

Fig. 8 Continued

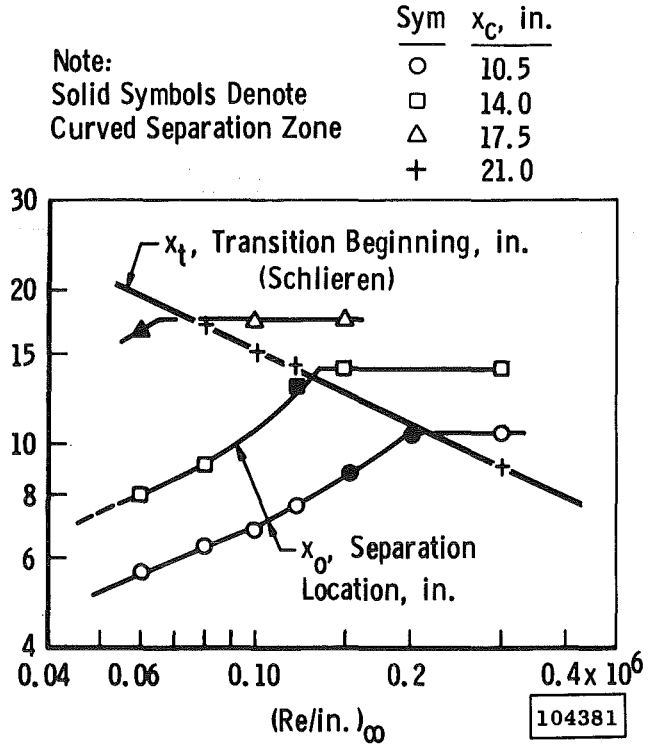

e. Hollow Cylinder, $M_\infty = 4$

Fig. 8 Concluded

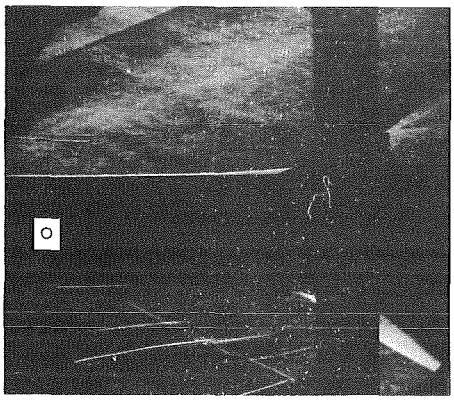

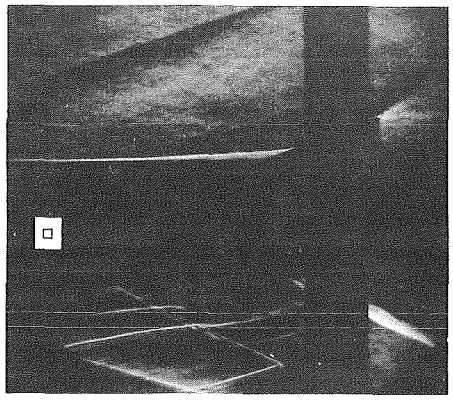

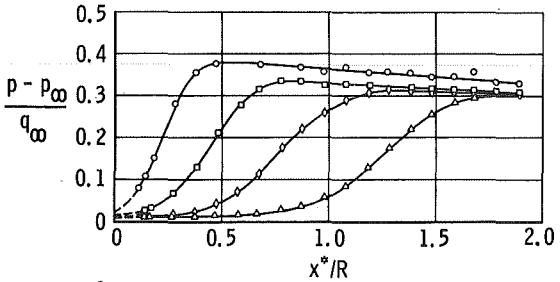

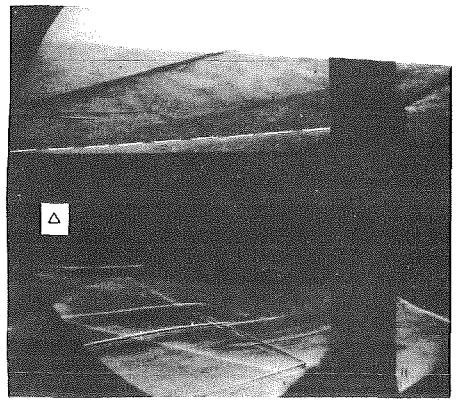

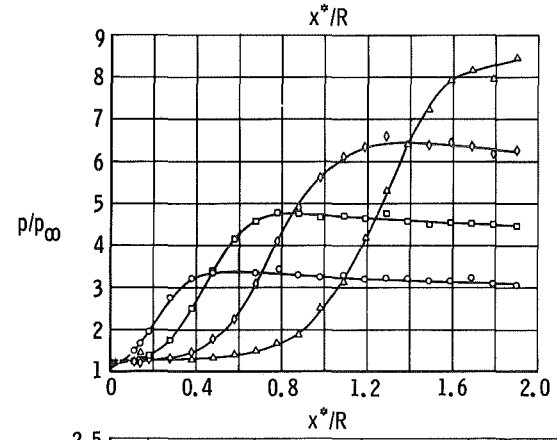

Sym	M_∞	$\Delta x_c/R$	$(Re/in.)_\infty \times 10^{-6}$
○	3	6.16	0.11
□	4	6.16	0.10
◇	5	6.16	0.10
△	6	6.16	0.11

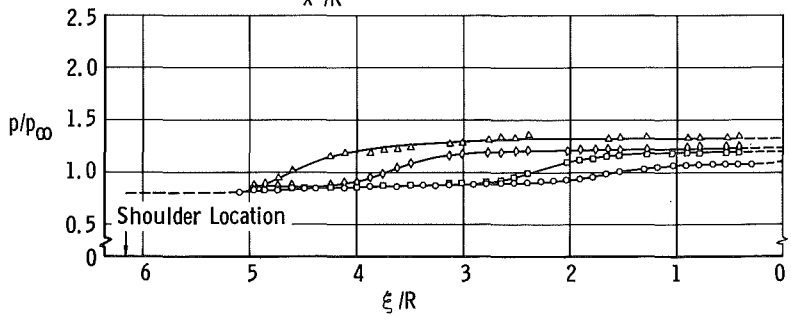

104382

a. 10-deg Sharp Cone, $(Re/in.)_\infty \simeq 0.1 \times 10^6$, R = 3.5

Fig. 9 Effect of Mach Number on Laminar Flow Separation Induced by a 20-deg Frustum

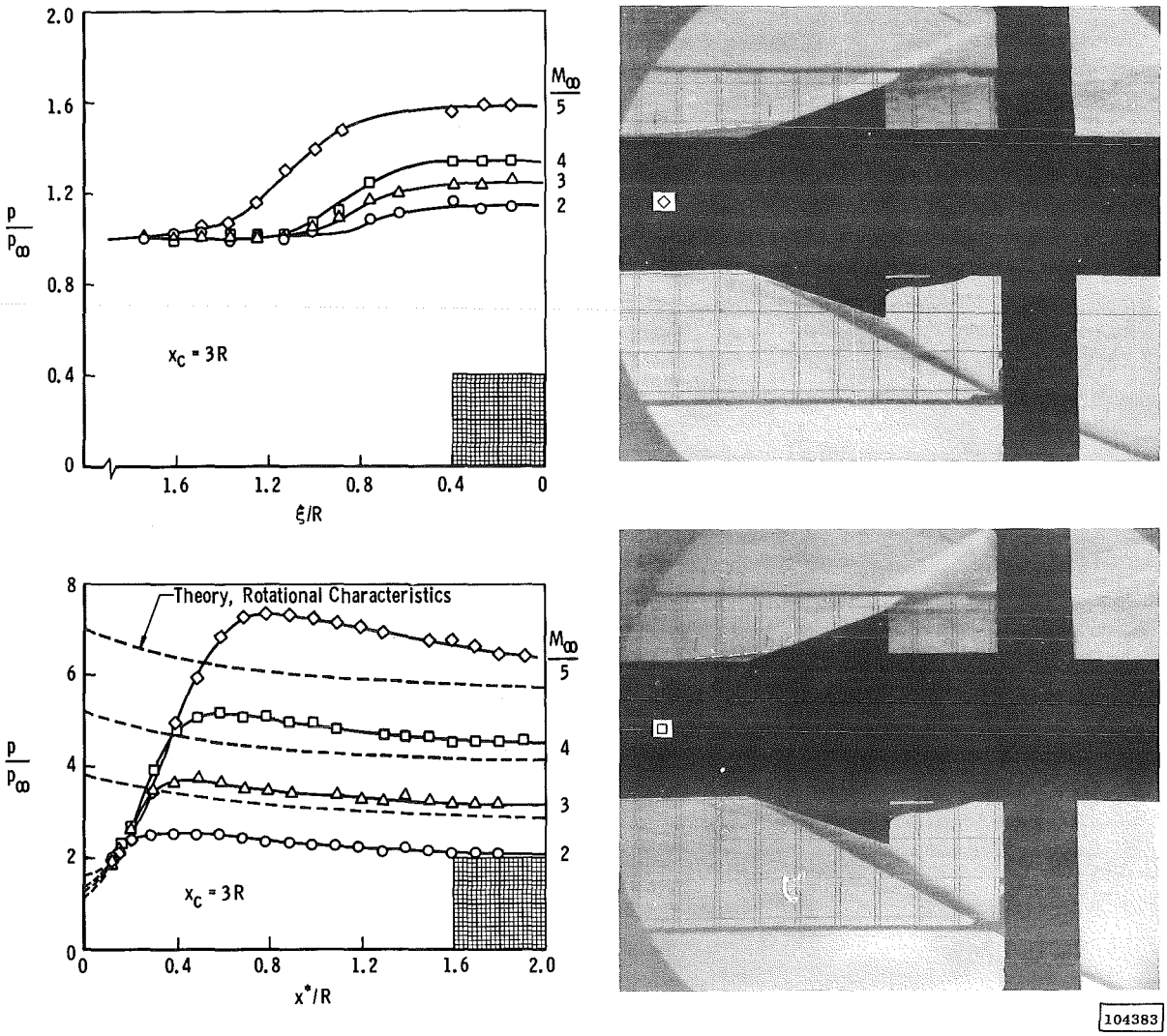

b. Hollow Cylinder, $(Re/in.)_\infty \simeq 0.1 \times 10^6$, R = 3.5 in.

Fig. 9 Continued

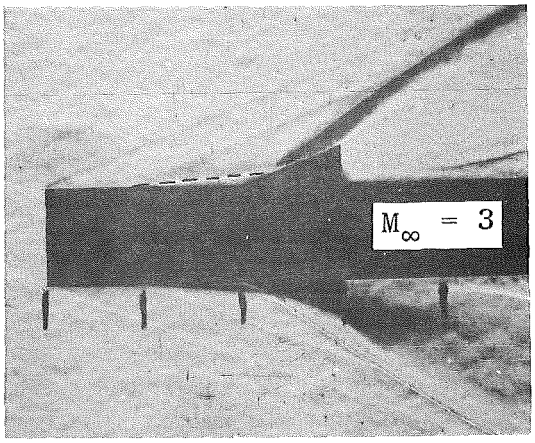

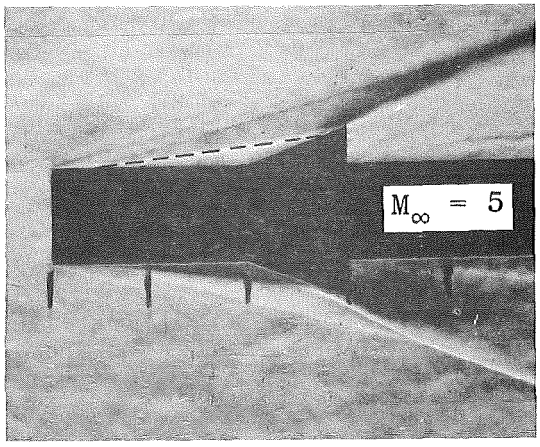

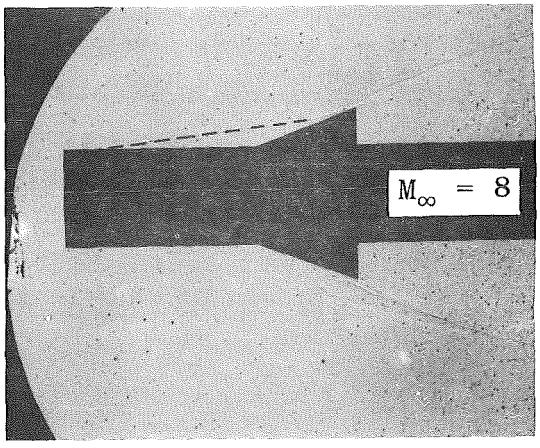

104384

c. Hollow Cylinder, $(Re/in.)_\infty \simeq 0.2 \times 10^6$, R = 0.5 in.

Fig. 9 Concluded

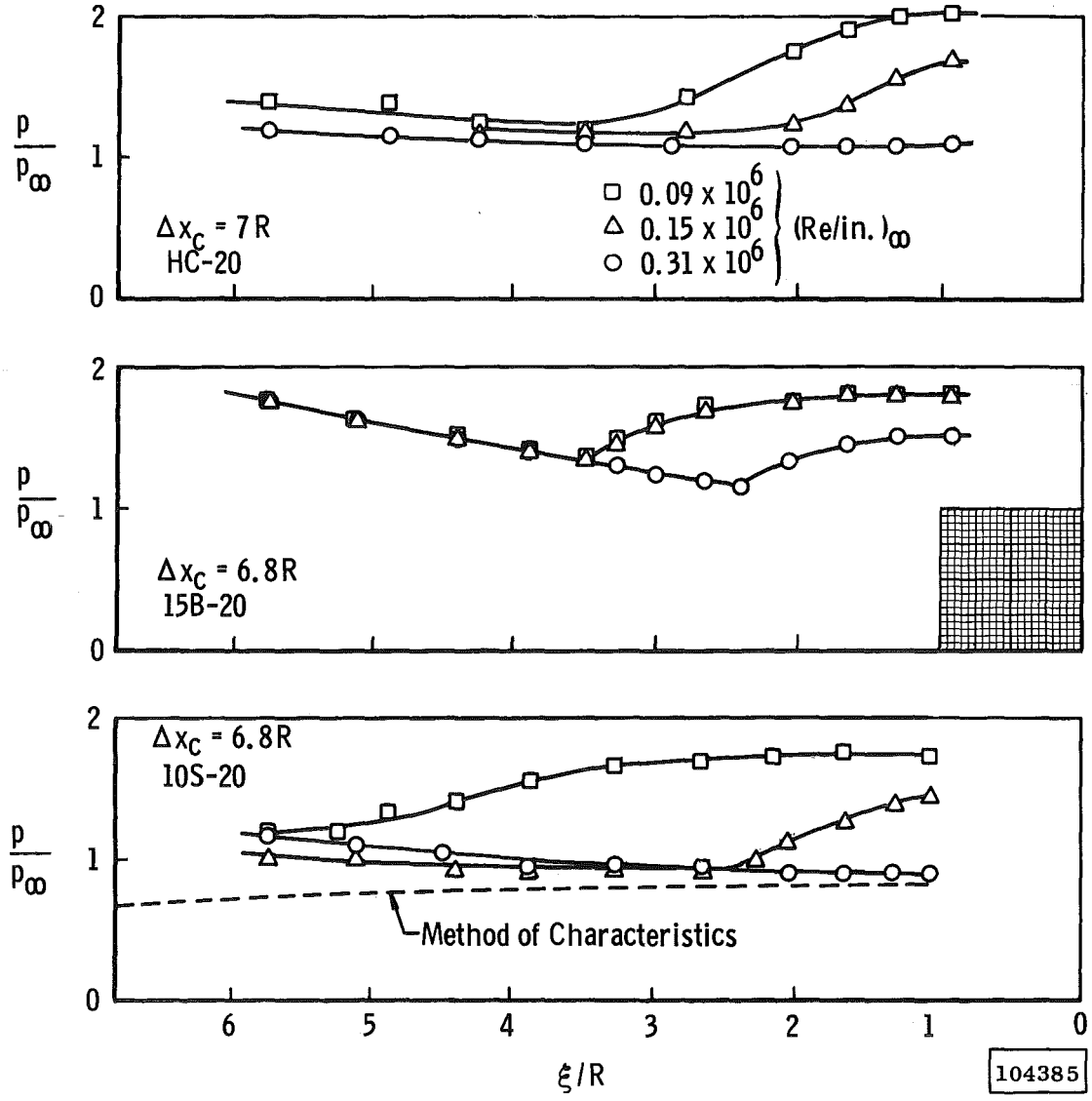

a. Cylinder Pressures

Fig. 10 Effect of Unit Reynolds Number on Pressure Distributions with Various Noses and a 20-deg Frustum at Mach 8, R = 3.5 in.

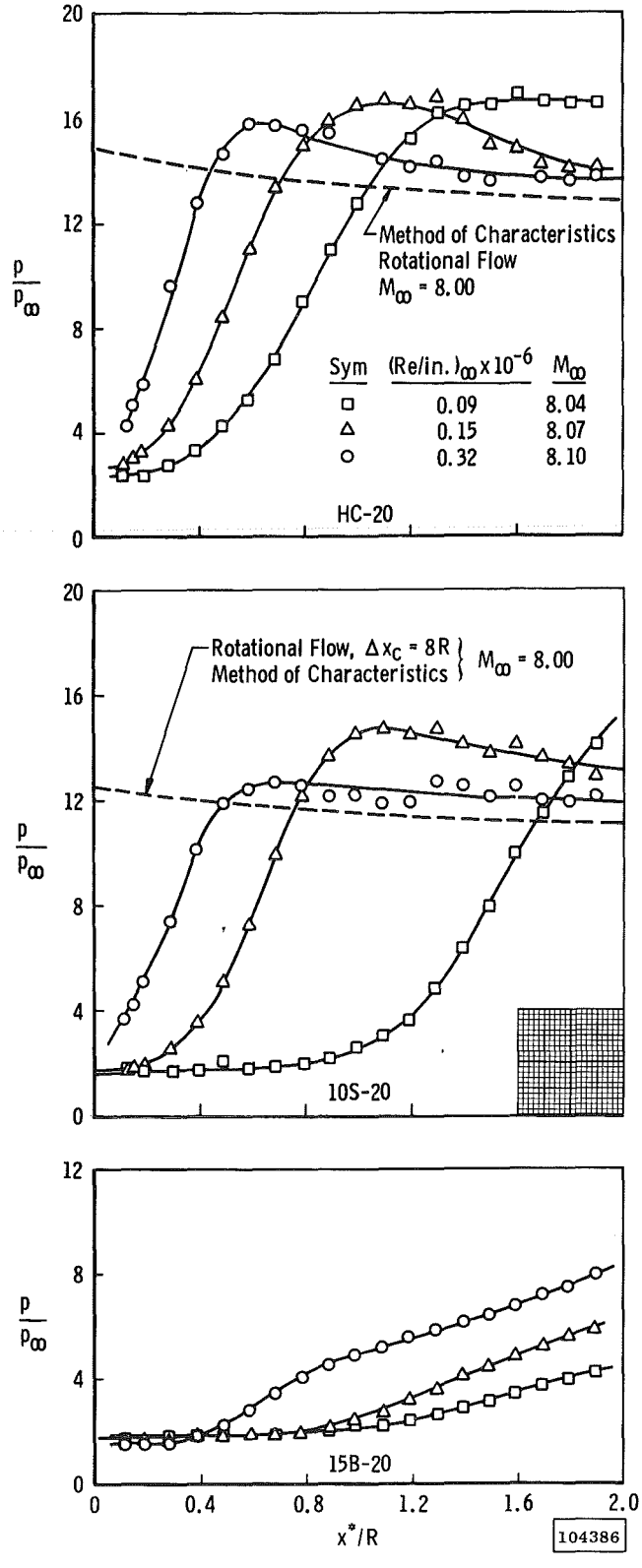

b. Frustum Pressures

Fig. 10 Concluded

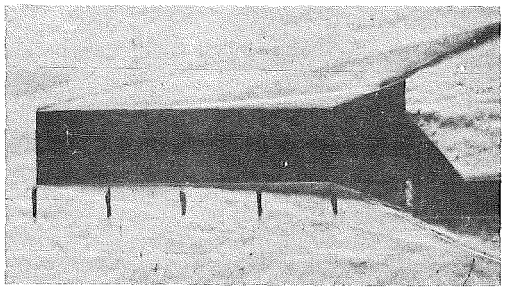

(1) $(Re/in.)_{\infty} = 0.30 \times 10^6$

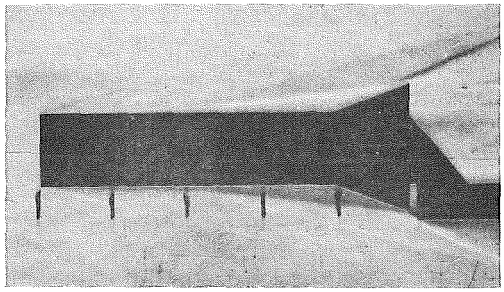

(2) $(Re/in.)_{\infty} = 0.10 \times 10^6$

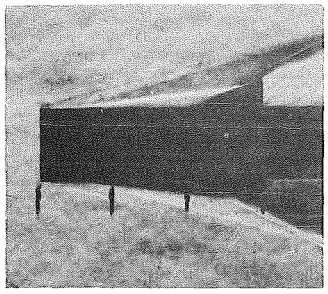

(3) $(Re/in.)_{\infty} = 0.30 \times 10^6$

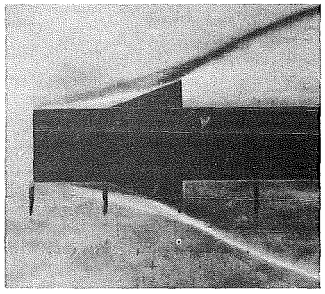

(4) $(Re/in.)_{\infty} = 0.30 \times 10^6$

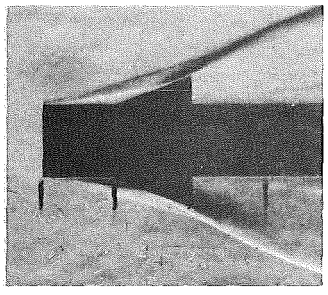

(5) $(Re/in.)_{\infty} = 0.15 \times 10^6$

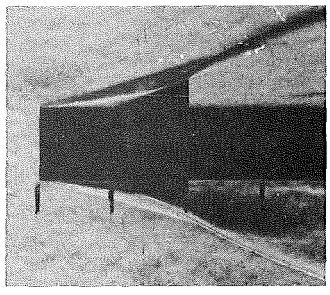

(6) $(Re/in.)_{\infty} = 0.10 \times 10^6$

104387

a. Schlieren Photographs

Fig. 11 Analysis of Schlieren Photographs for a Geometric Correlation of the Laminar Separation at Mach 5, Configuration HC-20, R = 0.5 in.

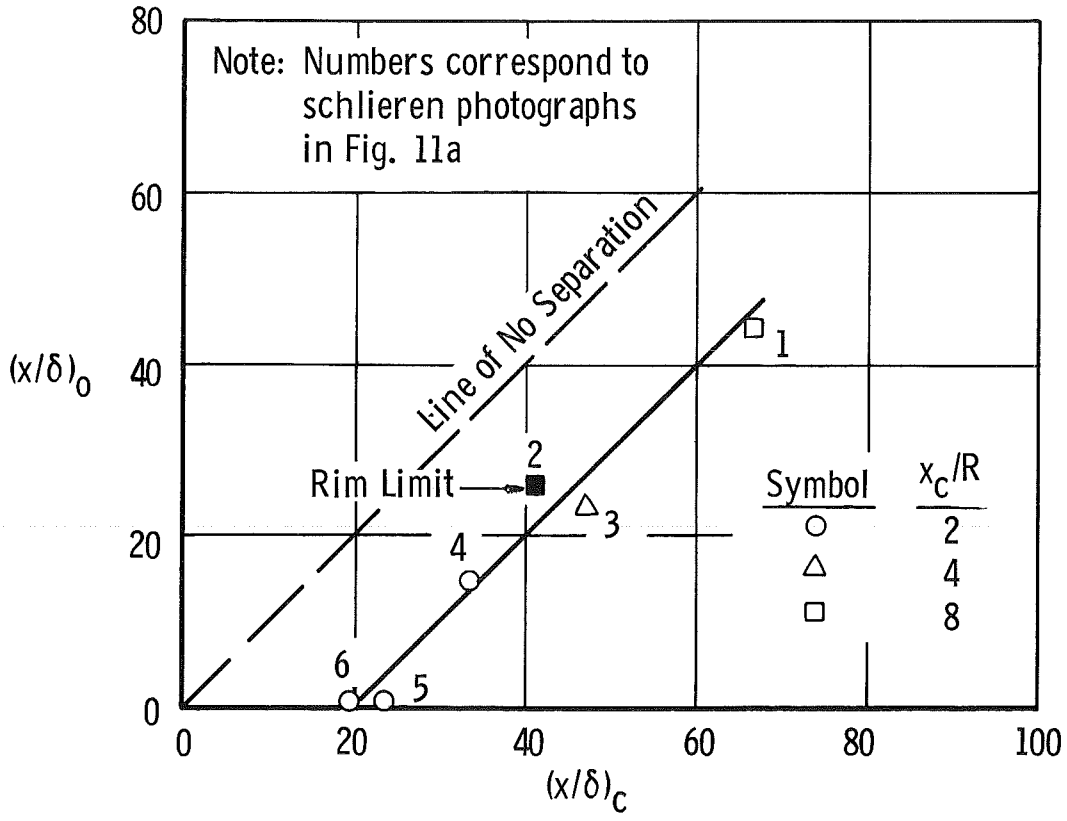

b. Separation Location versus Flare Location

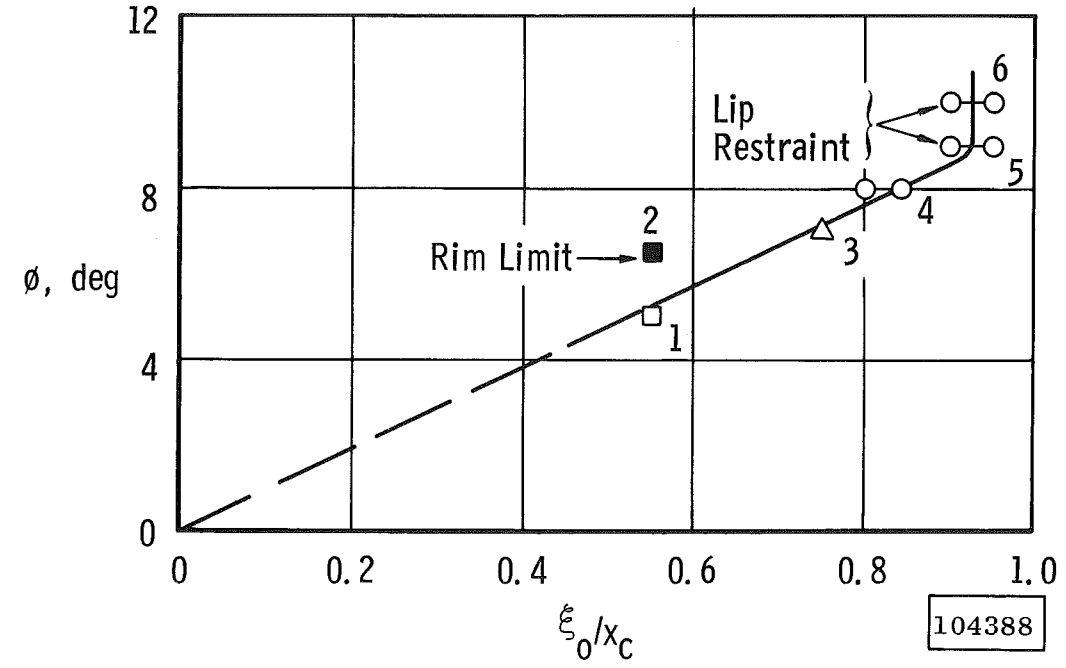

c. Lift-Off Angle versus Relative Extent of Separation

Fig. 11 Concluded

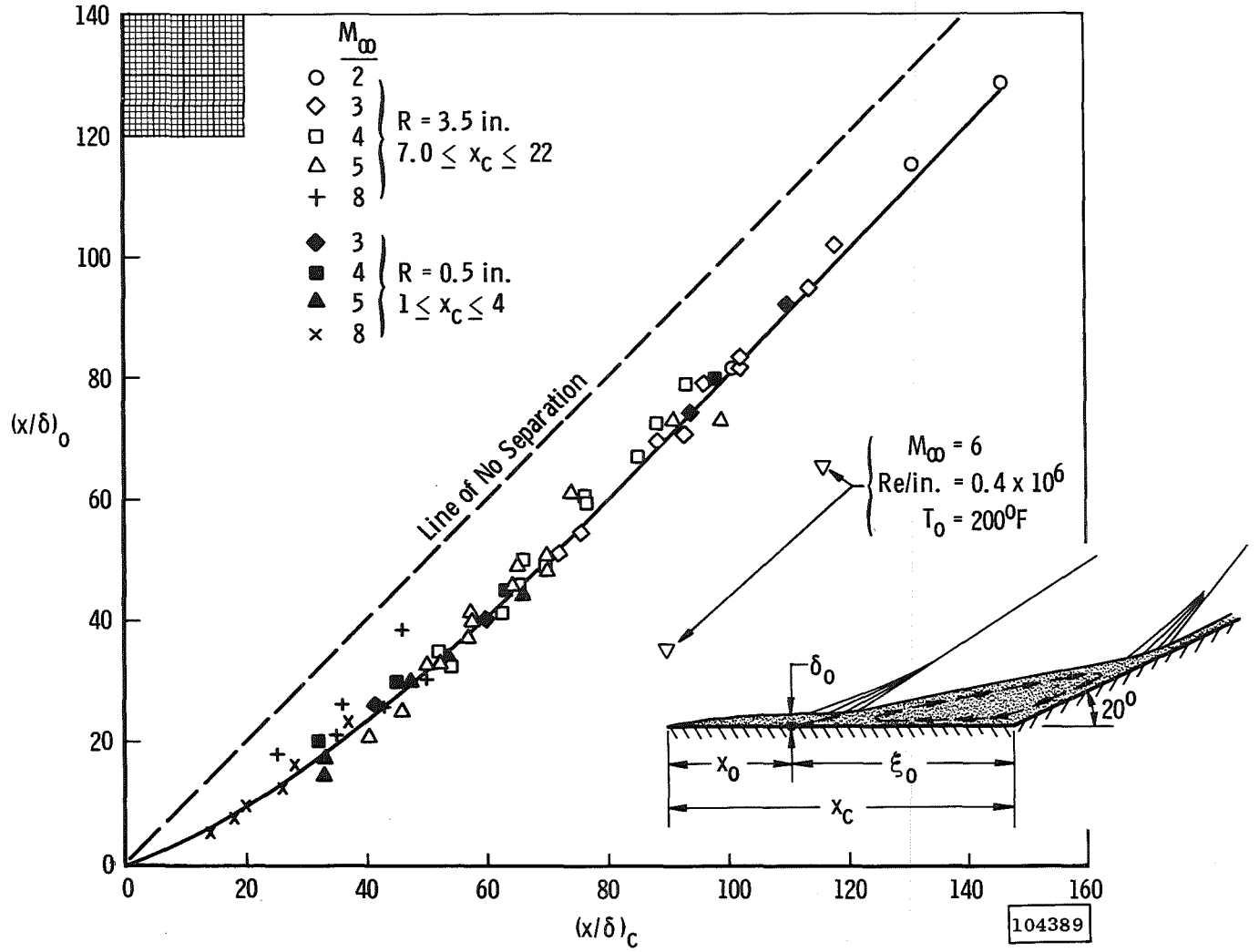

a. Hollow Cylinder

Fig. 12 Correlation of Laminar Separation Induced by a 20-deg Frustum at Supersonic and Hypersonic Speeds

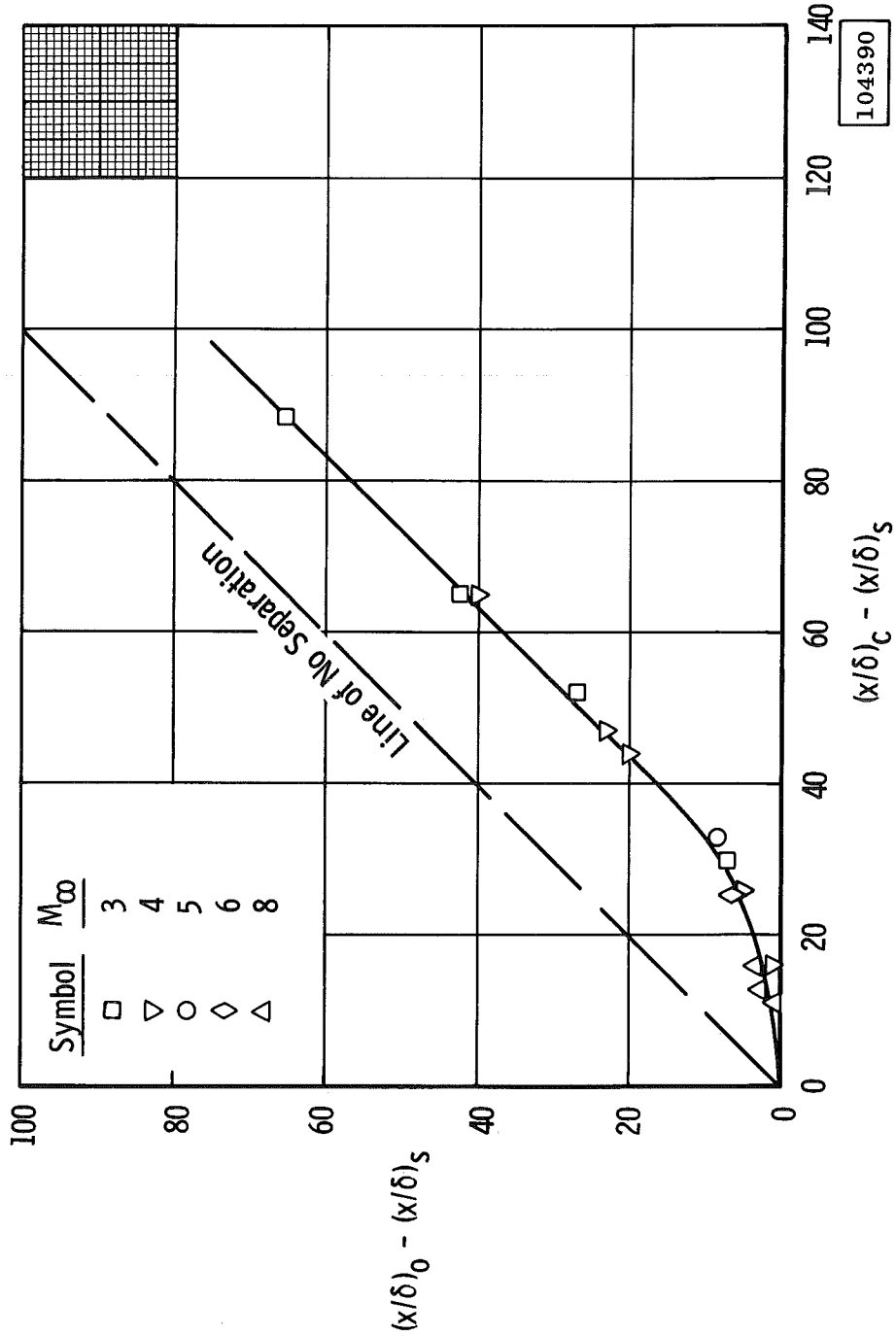

b. 10-deg Sharp Cone Cylinder

Fig. 12 Continued

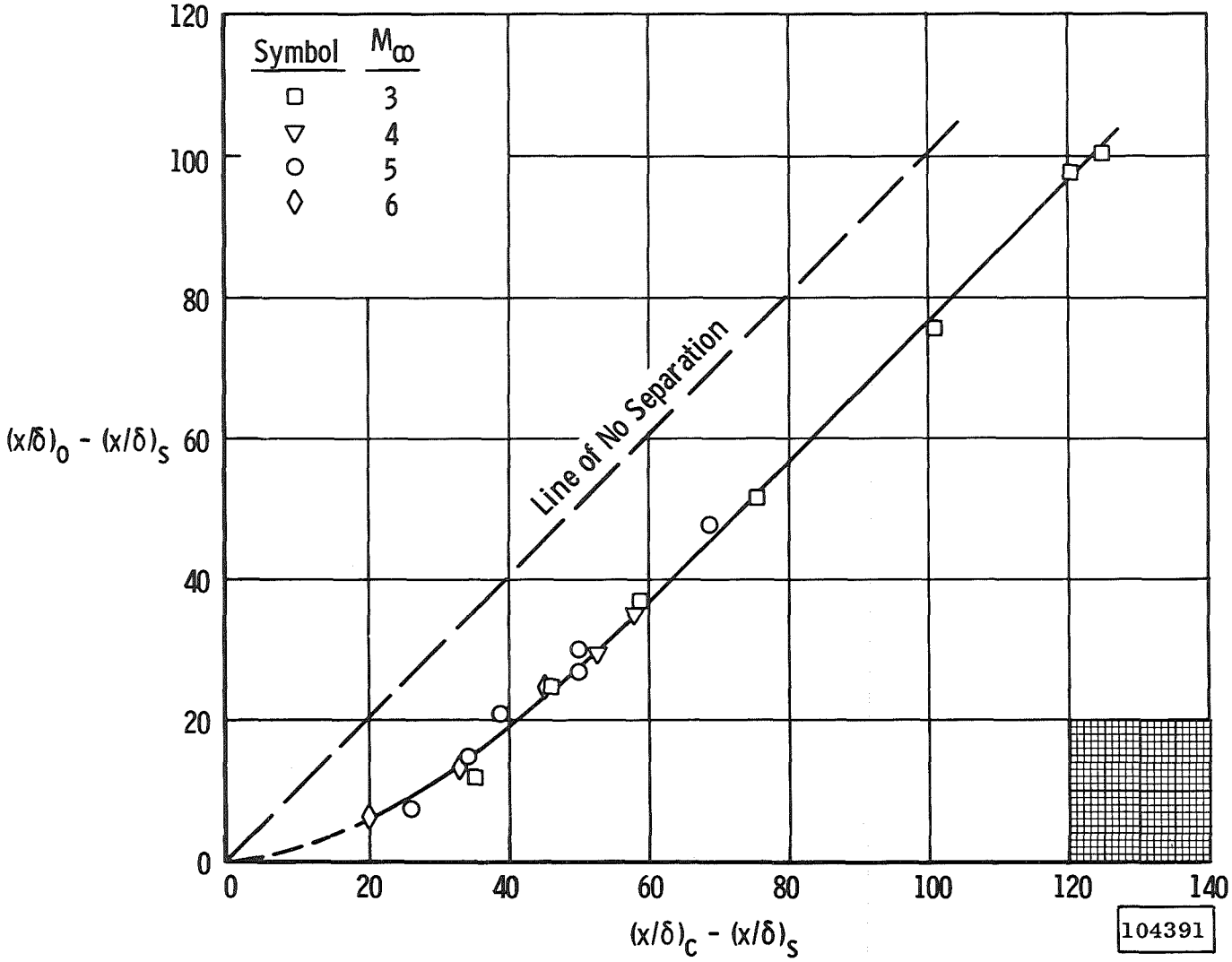

c. 15-deg Blunt Cone Cylinder

Fig. 12 Concluded

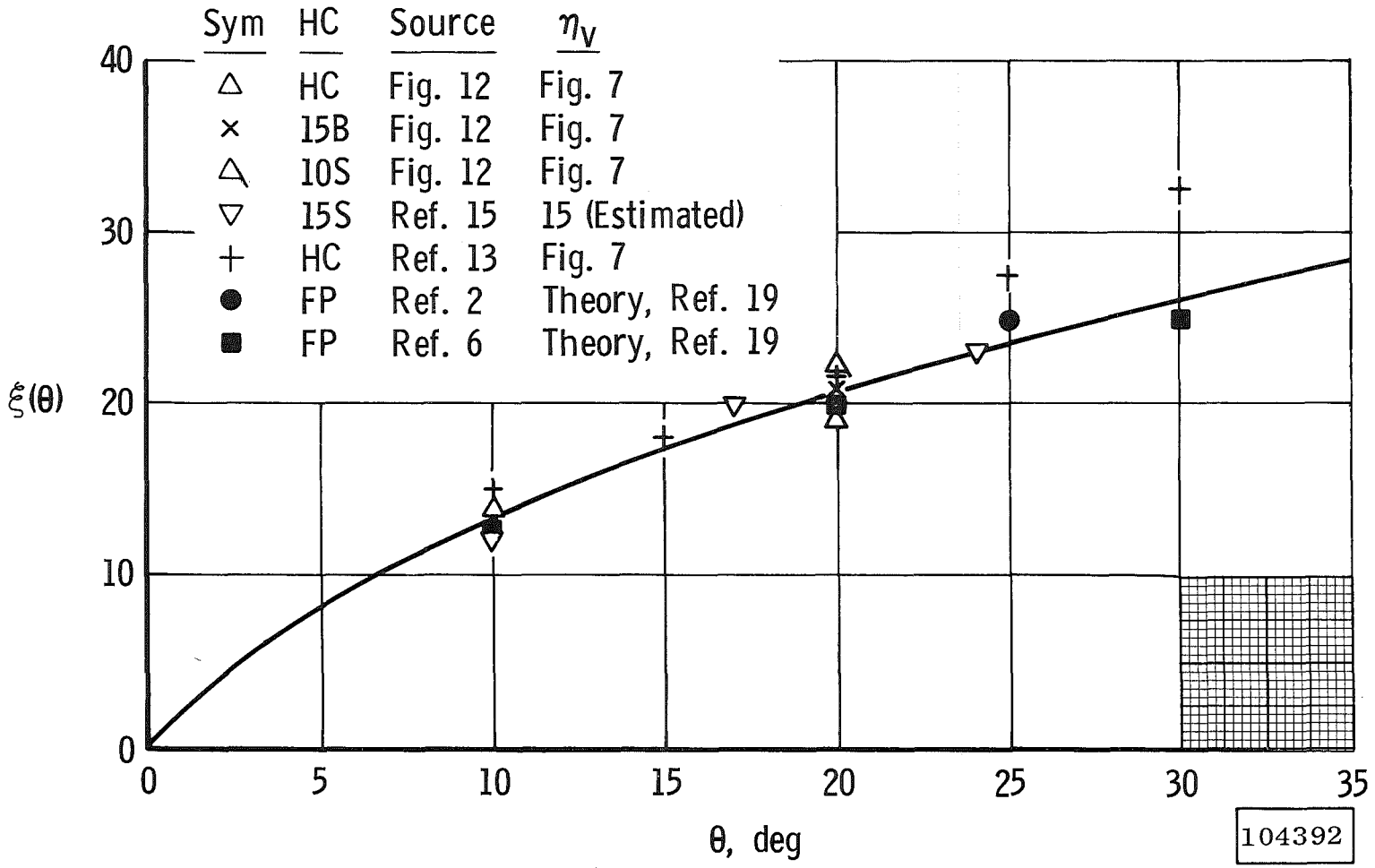

Fig. 13 Effect of Flare Angle on the Laminar Separation Extent Correlation Parameter

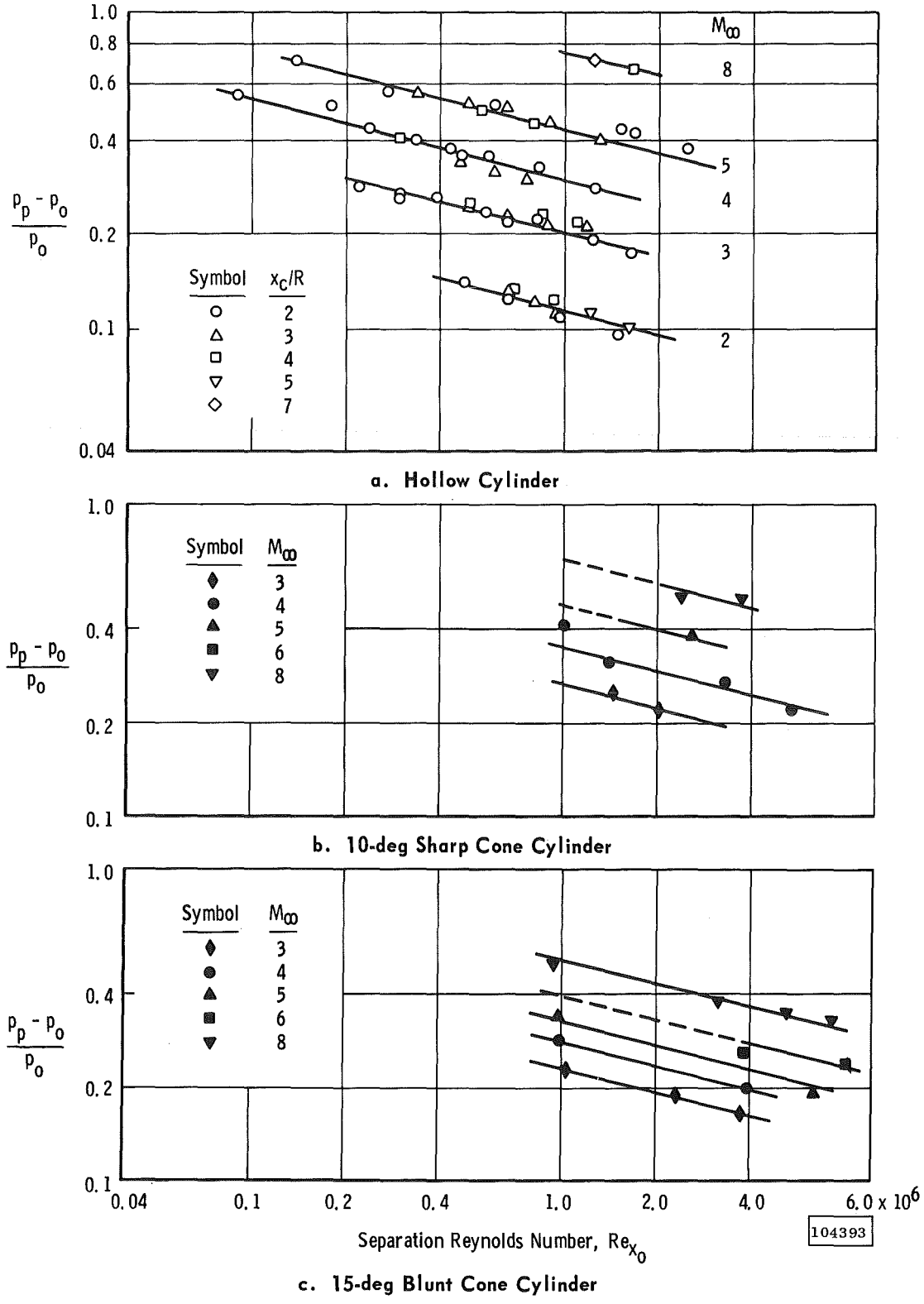

Fig. 14 Plateau Pressure Rise Variation with Separation Reynolds Number for Axisymmetric Configurations (θ = 20-deg)

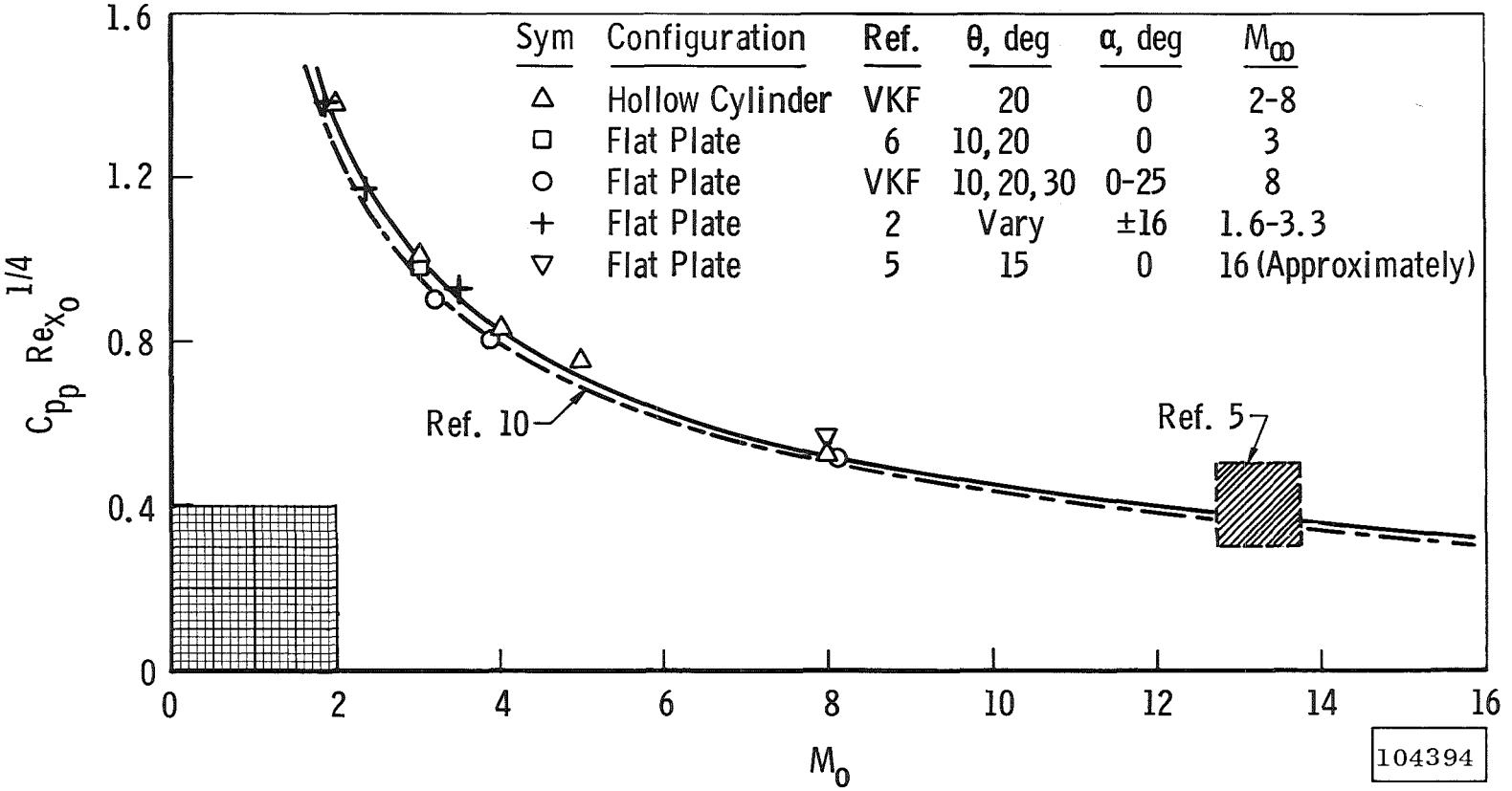

Fig. 15 Effect of Mach Number on Plateau Pressure Correlation for Two-Dimensional and Axisymmetric Flow